



HAL
open science

Deletion of fibroblast activation protein provides atheroprotection 1 2

Sokrates Stein, Julien Weber, Stefanie Nusser-Stein, Jürgen Pahla, Hui Zhang, Shafeeq Mohammed, Sara Oppi, Daniel S Gaul, Francesco Paneni, Anne Tailleux, et al.

► To cite this version:

Sokrates Stein, Julien Weber, Stefanie Nusser-Stein, Jürgen Pahla, Hui Zhang, et al.. Deletion of fibroblast activation protein provides atheroprotection 1 2. *Cardiovascular Research*, 2020, Online ahead of print. 10.1093/cvr/cvaa142 . inserm-02735410

HAL Id: inserm-02735410

<https://inserm.hal.science/inserm-02735410v1>

Submitted on 2 Jun 2020

HAL is a multi-disciplinary open access archive for the deposit and dissemination of scientific research documents, whether they are published or not. The documents may come from teaching and research institutions in France or abroad, or from public or private research centers.

L'archive ouverte pluridisciplinaire **HAL**, est destinée au dépôt et à la diffusion de documents scientifiques de niveau recherche, publiés ou non, émanant des établissements d'enseignement et de recherche français ou étrangers, des laboratoires publics ou privés.

1 **Abstract**

2 **Aims.** Fibroblast activation protein (FAP) is upregulated at sites of tissue remodelling including chronic
3 arthritis, solid tumours, and fibrotic hearts. It has also been associated with human coronary
4 atherosclerotic plaques. Yet, the causal role of FAP in atherosclerosis remains unknown. To investigate
5 the cause-effect relationship of endogenous FAP in atherogenesis, we assessed the effects of
6 constitutive *Fap* deletion on plaque formation in atherosclerosis-prone *apolipoprotein E* (*ApoE*) or *low-*
7 *density lipoprotein receptor* (*Ldlr*) knockout mice.

8 **Methods and results.** Using *en face* analyses of thoraco-abdominal aortae and aortic sinus cross-
9 sections, we demonstrate that *Fap* deficiency decreased plaque formation in two atherosclerotic mouse
10 models (-46% in *ApoE* and -34 % in *Ldlr* knockout mice). As a surrogate of plaque vulnerability fibrous
11 cap thickness was used; it was increased in *Fap*-deficient mice, whereas Sirius red staining
12 demonstrated that total collagen content remained unchanged. Using polarized light, atherosclerotic
13 lesions from *Fap*-deficient mice displayed increased FAP targets in terms of enhanced collagen
14 birefringence in plaques and increased pre-COL3A1 expression in aortic lysates. Analyses of the
15 Stockholm Atherosclerosis Gene Expression (STAGE) data revealed that *FAP* expression was
16 increased in human atherosclerotic compared to non-atherosclerotic arteries.

17 **Conclusions.** Our data provide causal evidence that constitutive *Fap* deletion decreases progression
18 of experimental atherosclerosis and increases features of plaque stability with decreased collagen
19 breakdown. Thus, inhibition of FAP expression or activity may not only represent a promising
20 therapeutic target in atherosclerosis but appears safe at the experimental level for FAP-targeted cancer
21 therapies.

22 **Translational Perspective**

23 Fibroblast activation protein (FAP) is upregulated at sites of chronic tissue remodelling including
24 rheumatoid arthritis and solid tumours. Indeed, depletion of FAP-positive cells inhibits tumour growth
25 by increasing antitumour immunity. FAP has also been correlated with human coronary plaques,
26 whereby its causal role remains unknown. Our data provide causal evidence that constitutive *Fap*
27 deletion decreases progression of experimental atherosclerosis and increases features of plaque
28 stability. Thus, inhibition of FAP expression or activity may not only represent a novel therapeutic target
29 for atherosclerosis but appears safe – at the experimental level – for FAP-targeted cancer therapies.

30

1 **1. Introduction**

2 Vulnerable plaques pose a central problem in human atherosclerosis. Their rupture may cause
3 complete thrombotic arterial lumen obstruction, which may lead to myocardial infarction or stroke. A
4 sufficiently thick fibrous cap ensures plaque stability and a barrier between blood and the prothrombotic
5 necrotic core within the plaque ^{1, 2}. Collagenases (e.g. matrix metalloproteinases (MMPs) and
6 cathepsins) degrade collagen within the fibrous cap, thereby thinning the cap and making them more
7 prone to rupture ³. Therefore, extra-cellular matrix-degrading collagenases have emerged as promising
8 therapeutic targets against rupture of vulnerable plaque ⁴. Interestingly, many collagenases involved in
9 tissue remodelling such as rheumatoid arthritis or tumour expansion play similar roles in atherogenesis
10 ^{3, 5}.

11 Fibroblast activation protein (FAP) can be membrane-bound or soluble, and is a constitutively active
12 serine protease that exhibits dipeptidyl peptidase IV activity and prolyl endopeptidase activity with a
13 specificity for collagens ⁶⁻⁸. Matrix turnover is a central event in the pathogenesis of chronic inflammatory
14 diseases such as rheumatoid arthritis, tumour formation and atherosclerosis. Along these lines, FAP is
15 expressed by activated fibroblasts in epithelial tumour stroma, arthritis and wound healing, but remains
16 virtually undetectable in healthy tissues ^{6, 9-11}. In rheumatoid arthritis, FAP is expressed in SMA-positive
17 myofibroblasts and associated with matrix metalloproteinase expression ⁹. Moreover, a recent study
18 showed that FAP was increased in cardiac fibrosis, which in turn promotes the development of various
19 cardiac diseases and heart failure ¹². Interestingly, engineered chimeric (FAP-)antigen receptor (CAR)
20 T cells could be used to target FAP in cardiac fibrosis; this strategy restored cardiac function in a
21 hypertensive heart failure model ¹².

22 Previously, we have reported that FAP expression is enhanced in human fibroatheromata versus
23 plaque-free aortae, and its expression increases upon plaque progression ¹³. Although expression of
24 FAP protein correlated with the macrophage burden in human aortic plaques, colocalization images
25 revealed that FAP was mainly expressed by smooth muscle cells ¹³.

26 Many collagenases involved in chronic tissue remodelling processes such as rheumatoid arthritis and
27 tumour progression play similar roles in atherogenesis ^{3, 5}. Yet, the causal role of FAP in atherogenesis
28 remains unknown. Therefore, we assessed the cause-effect relationship between the loss-of-function

1 of FAP and the phenotype of atherosclerosis by crossbreeding *Fap* knockout mice ¹⁴ with
2 atherosclerosis-prone *apolipoprotein E (ApoE)* or *low-density lipoprotein receptor (Ldlr)* knockout mice.

1 **2. Methods**

2

3 **2.1 Mice.** Mice with a germline *Fap* deletion were obtained from the Centenary Institute, Sydney, AU

4 ^{14, 15} and licensed from Boehringer Ingelheim Pharma GmbH & Co KG. Congenic C57BL6/J *Fap*^{-/-} and

5 *Fap*^{+/+} mice were kept in a temperature-controlled facility with a 12-h light/dark cycle and free access to

6 normal chow and water. To assess atherosclerosis development, *Fap*^{-/-} mice were crossbred to either

7 *Apoe*^{-/-} or *Ldlr*^{-/-} mice. Of those, male mice were fed a high-cholesterol diet (1.25% total cholesterol,

8 Research Diets) for 12 weeks starting at the age of 8 weeks. After being anesthetised with isoflurane

9 using a gas flow vaporizer (4.5 to 5% isoflurane) for 5 minutes, mice were euthanised by cardiac

10 puncture and exsanguination.

11 **2.2 Study approval.** All animal experiments were approved by the Veterinary Office of the Canton

12 Zurich (animal licenses: 189/2011 and 5263) and all procedures were in accordance to the guidelines

13 from Directive 2010/63/EU of the European Parliament on the protection of animals used for scientific

14 purposes.

15 **2.3 FAP activity assay.** The FAP specific enzyme assay was adapted from published assays ^{11, 16},

16 using 100 uM Z-Gly-Pro-aminomethylcoumarin (AMC) as substrate, and the prolyl endopeptidase

17 selective inhibitor S-17092 (Sigma-Aldrich #SML0181) at 0.1 uM to ensure FAP specificity.

18 **2.4 FAP proteomics.** Generation of *Fap*-deficient mouse embryonic fibroblasts and cultivation of the

19 cells was described previously ⁸. Terminal amine isotopic labelling of substrates (TAILS) and tests of

20 data significance were performed previously ⁸. The statistically significant cleavages in collagens were

21 arranged by location in primary structure and the cleavage sites that follow each Gly-Pro, the motif

22 typical of FAP mediated cleavage, were identified.

23 **2.5 Western blot analysis.** 30 mg aortic lysates were pulverized using a steel tissue grinder, and then

24 extracted in lysis buffer (50 mM Tris HCl pH 8.0, 125 mM NaCl, 0.25% NP-40, 0.5 mM

25 phenylmethylsulfonyl fluoride, and protease/phosphatase inhibitor cocktail) for 10 minutes. The

26 supernatant was transferred, and the protein content measured using Bradford reagent. Before

27 running SDS-PAGE, protein lysates were boiled for 5 min at 95°C. Following proteins were used for

28 Western blotting: anti-COL3A1 (22734-1-AP, Proteintech), anti-COL2A1 (sc-52658, Santa Cruz), anti-

29 COL1A1 (PA1-26204, Invitrogen), anti- α tubulin (sc-8035, Santa Cruz), anti- β actin (sc-47778, Santa

30 Cruz), and anti-GAPDH (TA802519, Origene).

1 **2.6 Plasma lipid analysis.** Total cholesterol (TC) and triglyceride (TG) plasma concentrations were
2 measured using an enzymatic colorimetric assay (Biomerieux). To obtain lipoprotein fractions for fast-
3 protein liquid chromatography (FPLC) analysis, each individual plasma sample was loaded on a
4 filtration chromatography column onto a Superose 6 10/300 GL column (GE Healthcare), which allows
5 separation of the three major lipoprotein classes (VLDLs, LDLs, HDLs and free glycerol) according to
6 their size. Cholesterol and triglyceride concentrations were continuously measured in the effluent using
7 an enzymatic colorimetric assay (Biomerieux) and results are expressed as O.D.

8 **2.7 Immunohistochemistry.** The heart-aortic root samples were stored in optimal cutting temperature
9 (OCT) compound at -80°C, and then cut with a cryostat set at -20°C. The samples were then cut from
10 the left ventricular basis towards the aortic valves. Once reaching the cusps, the specimen was re-
11 orientated to achieve stringent cross-sectional cutting. 5 µm thick serial cross sections were then
12 collected at approximately 100 µm intervals on microscopic glass slides until the aortic cusps were no
13 longer visible. These 5 µm-thick serial cryosections were stained with Oil-red O (ORO), rat anti-CD68
14 (MCA 1957GA, Serotec), rat anti-CD3 (MCA 500GA, Serotec), rat anti-VCAM-1 (MCA 1129, Serotec),
15 and rabbit anti-αSMA (D4K9N, Cell Signaling). Means were taken from at least 6 different mice
16 evaluating at least 6 serial cryosections/tissue from each mouse. Thoraco-abdominal aortae were
17 fixed with 4% paraformaldehyde and plaques stained with Oil-red O. Collagen content, fibrous cap
18 thickness, and necrotic core size were analysed by Elastica van Gieson staining. Sirius Red stainings
19 were performed to visualize collagen content under normal light.

20 **2.8 Second harmonics.** 5-µm-thick serial cryosections from the aortic sinus were used to perform
21 second-harmonic generation of collagen fibers using two-photon microscopy. Second-harmonic signal
22 was generated by tuning the Mai Tai Ti:sapphire laser to 880 nm and collecting the resultant tissue
23 emission at 440 nm.

24 **2.9 Gene expression analysis.** Aortic RNAs were extracted using TRIZOL (Thermo Fisher, no.
25 15596026). For RT-qPCR, cDNA was generated using the All-in-One cDNA Synthesis kit (Biotool, no.
26 B24403), and analysed by qPCR using a SYBR Green qPCR Master Mix (Biotool, no. B21202) and the
27 primers listed in the online supplement (**Supplemental Table S4**). Expression data were normalized to
28 housekeeping genes, i.e. *Actb*, *B2m* and/or *Ppib* mRNA levels.

1 **2.10 Transcriptomic data analyses.** The raw and/or normalized transcriptomic data from previous
2 studies are publicly available on Gene Expression Omnibus (GEO; www.ncbi.nlm.nih.gov/geo) under
3 the accession number GSE40231 (STAGE¹⁷) and analysed as described previously¹⁸. The *tabula muris*
4 data can be accessed and analysed online (<https://tabula-muris.ds.czbiohub.org>). The single cell-RNA
5 seq data was obtained from Prof. Qinbo Xu from the King's College London British Heart Foundation
6 Centre (United Kingdom).¹⁹

7 **2.11 Statistics.** Data are presented as scatter plots plus mean. Comparison of differences between
8 two groups was assessed using unpaired two-tailed Student's *t*-tests. A nonparametric Mann-Whitney
9 test was used for the analysis of the SGH data since the data distribution did not pass the D'Agostino
10 & Pearson omnibus normality test. Multiple group comparisons were assessed by ANOVA analysis and
11 Bonferroni post-hoc tests, and multiplicity adjusted P values are displayed for the comparisons.
12 Differences of $p < 0.05$ were considered statistically significant. Statistical analyses were performed
13 using GraphPad Prism 6.

1 3. Results

2 3.1 Deletion of *Fap* protects against atherosclerosis

3 To address the causal role of endogenous FAP in atherogenesis, we crossbred *Fap*-deficient mice¹⁵
4 with two different atherosclerosis-prone mouse models, i.e. *Ldlr*^{-/-} and *Apoe*^{-/-} mice²⁰ (**Supplemental**
5 **Figure 1**). Deletion of FAP was assessed by genotyping and confirmed by measuring its enzymatic
6 activity: FAP activity was abolished in both mouse models with constitutive *Fap* deletion (**Figure 1A,**
7 **B**). We next placed 8-week old male mice on a high-cholesterol diet for 12 weeks and assessed
8 atherosclerotic plaque development. Deletion of *Fap* diminished formation of atherosclerotic lesions by
9 approximately one third in *Ldlr*^{-/-} *Fap*^{-/-} and by about half in *Apoe*^{-/-} *Fap*^{-/-} mice (**Figure 1C, D**). While
10 *Apoe*^{-/-} *Fap*^{-/-} were slightly heavier than control *Apoe*^{-/-} *Fap*^{+/+} mice, no difference in body weight was
11 noted in the *Ldlr*^{-/-} background (**Supplemental Figure 2**).

12 We next examined whether plasma levels of total cholesterol and triglycerides at the time of harvesting
13 correlated with the atherosclerosis phenotype. Total cholesterol content did not differ in any of the two
14 atherosclerotic mouse models, while plasma triglyceride levels were increased in
15 *Apoe*^{-/-} *Fap*^{-/-} but not in *Ldlr*^{-/-} *Fap*^{-/-} mice (**Supplemental Figure 3**). Hematological analyses did not
16 reveal differences in the number of leukocytes subpopulations, erythrocytes or platelets between
17 *Ldlr*^{-/-} *Fap*^{-/-} and *Ldlr*^{-/-} *Fap*^{+/+} mice (**Supplemental Table 1**). On the other side, *Apoe*^{-/-} *Fap*^{-/-} had a
18 reduced amount of blood neutrophils and platelets, and an increased number of monocytes compared
19 to *Apoe*^{-/-} *Fap*^{+/+} controls. *Apoe* knockout mice on a high-cholesterol diet display a stronger pro-
20 inflammatory and atherogenic phenotype compared with *Ldlr*^{-/-} mice²⁰, which could be related to the
21 differences observed in leukocyte subpopulations (**Supplemental Table 1**).

22 3.2 *Fap*-deletion increases protective fibrous cap thickness

23 To better characterize the atherosclerotic lesions, we carried out several immunohistochemical
24 stainings on cross-sections of the aortic sinus of *Apoe*^{-/-} *Fap*^{-/-} and *Apoe*^{-/-} *Fap*^{+/+} mice. Along with the
25 reduced number of thoraco-abdominal lesions, *Apoe*^{-/-} *Fap*^{-/-} mice displayed reduced content of neutral
26 lipids in the aortic sinus compared to *Apoe*^{-/-} *Fap*^{+/+} mice (**Figure 2A and Supplemental Figure 4**).
27 Interestingly, we did not observe any difference in the amount of the vascular cell adhesion molecule 1
28 (VCAM-1), macrophages (CD68⁺ cells), or T cells (CD3⁺ cells) between the two genotypes (**Figure 2B**

1 – D). These findings suggest that the atherosclerotic phenotype is not secondary to a differential
2 accumulation of immune cells within the lesions.

3 Since FAP is an extra-cellular matrix-degrading collagenase, we performed Elastica van Gieson
4 stainings to measure the content of collagen and to assess advanced plaque parameters in aortic sinus
5 cross-sections. Surprisingly, there was no significant difference in the content of collagen in *Apoe*^{-/-} *Fap*^{-/-}
6 ^{-/-} compared to *Apoe*^{-/-} *Fap*^{+/+} mice (**Figure 3A**). However, atherosclerotic lesions from *Apoe*^{-/-} *Fap*^{-/-} mice
7 displayed larger fibrous caps, whereas the size of the necrotic cores was comparable to *Apoe*^{-/-} *Fap*^{+/+}
8 mice (**Figure 3B-D**), suggesting that *Apoe*^{-/-} *Fap*^{-/-} mice do not only develop less atherosclerosis, but
9 their lesions are also less prone to rupture. α -smooth muscle actin (α -SMA) staining showed a trend for
10 increased vascular smooth muscle cell content within the atherosclerotic lesions, suggesting that
11 vascular smooth cells migrated into the plaques to reinforce the fibrous cap (**Supplemental Figure 5**).

12 **3.3 Altered collagen organization in aortic sinus lesions from *Fap*-deficient mice**

13 We next performed Sirius red stainings as a alternative method to quantify the collagen content. It
14 confirmed that there is no difference in collagen content between the genotypes (**Figure 3E**).
15 Previously, Santos et al. showed that tumours from *Fap*-deficient mice (with a LacZ knockin, *Fap*^{lacZ/lacZ})
16 display increased collagen birefringence under polarised light in comparison to wildtype mice ²¹,
17 suggesting a reduced organization of the collagen fibers. To investigate a possible change in collagen
18 organization, we performed second-harmonic generation (SHG) of collagen on aortic sinus lesions
19 using two-photon microscopy laser microscopy ^{22, 23}. These analyses revealed that lesions of *Apoe*^{-/-}
20 *Fap*^{-/-} mice displayed increased SHG signals compared to *Apoe*^{-/-} *Fap*^{+/+} mice (**Figure 3F**), confirming
21 that deletion of FAP indeed augments the deposition of fibrillar collagens in these lesions.

22 **3.4 Proteomic analysis demonstrates that FAP cleaves several collagens**

23 To investigate the underlying mechanisms, we first analysed the expression of collagens, extracellular
24 matrix proteases and fibrosis markers in the aortae. Despite a trend for increases fibrosis markers, we
25 observed no significant difference of the transcripts at mRNA level (**Supplemental Figure 6**). In order
26 to understand how FAP induces the observed changes in collagen structure, we drilled down into our
27 targeted proteomic analyses of cell culture supernatants from *Fap*^{-/-} mouse embryonic fibroblasts to
28 identify potential collagen targets of FAP. We had found by stable isotope labelling with amino acids in
29 cell culture (SILAC) that the quantities of collagens 3, 5 and 6 differed in the presence of enzymatically

1 active FAP compared to inactive FAP⁸. In addition, terminal amine isotopic labelling of substrates
2 (TAILS) showed that the major collagen species COL1A1, COL1A2, COL5A2 and COL3A1 are
3 proteolytic targets of FAP in murine fibroblast cultures. The multiple cleavage sites in these
4 precollagens are probably generated co-operatively by FAP with other collagenases⁸. However, we
5 found that many of these cleavage sites followed Gly-Pro, which is prototypical of FAP-induced
6 hydrolysis, and that most of the greatest increases in collagen fragmentation were coincident with
7 cleavage after Gly-Pro (**Figure 4A-D**).

8 **3.5 Reduced cleavage of pre-COL3A1 in *Fap* knockout mice**

9 To validate the SILAC-TAILS data and verify if collagen degradation could also be affected in the *Fap*-
10 deficient mice, we analysed the protein expression of the three main collagens in aortic lysates of
11 *Apoe*^{-/-} *Fap*^{-/-} and *Apoe*^{-/-} *Fap*^{+/+} mice. Interestingly, we observed an increase of the precursor of
12 COL3A1 in *Apoe*^{-/-} *Fap*^{-/-} compared to *Apoe*^{-/-} *Fap*^{+/+} aortae (**Figure 4E, F, and Supplemental Figure**
13 **7A**), suggesting that the precursor cannot be properly cleaved in FAP-deficient mice. Conversely,
14 COL1A1 and COL2A1 products were not altered between the two genotypes (**Supplemental Figure**
15 **7C-F**). Noteworthy, there is no known molecular basis for this preference of FAP for COL3 over other
16 collagen subtypes.

17 **3.6 Pathway analyses of FAP-expressing cells supports its role in collagen remodelling**

18 Previously studies showed that FAP is mainly expressed in fibroblast and vascular smooth muscle cells.
19 Analysis of the transcriptome of targeted aortic fluorescent activated cell sorting (FACS)-isolated aortic
20 cell available at *Tabula muris*²⁴ showed and confirmed that FAP is mainly expressed by fibroblasts
21 (**Supplemental Figure 8**). Since these were aortae from non-atherosclerotic mice, we further analysed
22 an untargeted single cell RNA-sequencing dataset from aortae of *Apoe* knockout mice¹⁹. We first
23 selected all cells displaying *FAP* sequencing counts (>2), and then filtered the top 20 highest expressed
24 transcripts of each of these cells (**Supplemental Table S2**). Interestingly, pathway analysis shows
25 enrichment of extracellular remodelling, such as collagen and extracellular fibril organisation,
26 extracellular matrix and exosome, and collagen binding (**Supplemental Table S3**).

27

28

29 **3.7 Increased expression of *FAP* in human atherosclerotic vessels**

1 To evaluate whether the expression of FAP could be altered in human atherosclerotic plaques
2 compared to healthy arteries, we compared the expression of *FAP* in atherosclerotic aortic roots to non-
3 atherosclerotic mammary arteries from the Stockholm Atherosclerosis Gene Expression (STAGE)¹⁷
4 study. Atherosclerotic aortae revealed an increased expression of *FAP* as compared to non-
5 atherosclerotic mammary arteries (**Figure 4G**). Together, these data suggest that *FAP* expression is
6 increased in human atherosclerotic plaques and could be a promising target for pharmacologic
7 inhibition.

1 4. Discussion

2 In a previous study, we demonstrated that FAP expression is increased in human fibroatheromata
3 versus plaque-free aortae, and that its expression positively correlates with the stages of plaque
4 progression¹³. Moreover, soluble FAP cleaves α 2-antiplasmin, which enhances its activity and
5 incorporation into fibrin clots, thus promoting coagulation²⁵. Surprisingly, the levels of circulating FAP
6 are reduced in patients with coronary artery disease or stroke²⁶⁻²⁹, and suggest that tissue resident and
7 circulating FAP are independent markers of cardiovascular diseases³⁰.

8 The current study provides the following novel findings (**Figure 5**):

9 1) Constitutive genetic *Fap* loss-of-function in atherosclerosis-prone *Apoe* or *Ldlr*-deficient mice
10 decreases plaque formation that is independent of plasma lipid levels. Moreover, the content of plaque
11 VCAM-1, macrophages, and T cells was not different between the groups.

12 2) *Fap* deletion increases features of plaque stability with increased fibrous cap thickness. Analyses of
13 aortic roots demonstrated that atherosclerotic lesions from *Apoe*^{-/-} *Fap*^{-/-} mice harbour thicker fibrous
14 caps.

15 3) Plaque matrix analyses display increased SHG signals compared to *Apoe*^{-/-} *Fap*^{+/+} mice. The
16 enhanced SHG signal suggests that the deletion of *Fap* increases deposition of fibrillar collagens in the
17 lesions.

18 Using a targeted proteomic analyses of cell culture supernatants from *Fap*^{-/-} mouse embryonic
19 fibroblasts that express enzymatically active FAP or inactive FAP, we showed that FAP cleaves major
20 collagens species at several sites, including COL3A1. When analysing COL3A1 protein expression in
21 aortic lysates, we detected reduced cleavage of pre-COL3A1 in *Apoe*^{-/-} *Fap*^{-/-} compared to *Apoe*^{-/-} *Fap*^{+/+}
22 mice. Notably, in a recent study with acromegaly patients, surgical or medical treatment of the pituitary
23 somatotroph tumour markedly reduced the levels of FAP compared to untreated subjects. These effects
24 were closely associated with a reduction in biomarkers of collagen turnover³¹.

25 The exact mechanisms by which impaired COL3A1 expression and/or processing affect collagen fibril
26 organization is not yet well known. In the first *Col3a1* knockout study, Rudolph Jaenisch's group
27 demonstrated that collagen SHG imaging of fibroblast-derived matrices showed that *Col3*-deficient
28 fibroblasts produced a more aligned and fibrillar matrix than wild-type cells, and that COL3A1 is crucial

1 for collagen I fibrillogenesis ³². Therefore, changes in COL3A1 processing have an impact on the
2 formation of fibrillar collagens.

3 Moreover, the vascular (type IV) form of the Ehlers-Danlos Syndrome, which is caused by mutations in
4 the *COL3A1* gene, leads to an impaired fibrillar collagen disposition ³²⁻³⁶. Both exon-skipping or
5 missense mutations in the *COL3A1* loci can disrupt the collagen triple helix. These malformed helices
6 are then degraded or accumulate in intracellular compartments, and hence not secreted into the
7 extracellular matrix. As a consequence, the reduction in COL3A1 caused by the mutations alters the
8 size and structure of collagen fibrils ³⁴. Nevertheless, the precise mechanisms by which mutant COL3A1
9 causes dermal and vascular fragility remain largely unexplored.

10 Taken together, our current mouse and published human data ¹³ demonstrate that endogenous pro-
11 oncogenic FAP promotes atherosclerosis development. Interestingly, depletion of FAP-positive cells
12 inhibits tumour growth by increasing antitumour immunity ²¹, and small antagonists and blocking
13 antibodies for FAP are already being applied in oncology ³⁷. Along these lines, it will not only be exciting
14 to further test the impact of FAP inhibition on atherosclerosis in the experimental and clinical setting,
15 FAP targeting may also comprise a promising cardio-oncological treatment avenue.

16 Interestingly, a recent study suggest that FAP also plays a central role in cardiac fibrosis, which
17 promotes the development of various cardiac diseases and heart failure ¹². The authors showed that
18 engineered chimeric FAP-antigen receptor T cells can be used to reduce experimental cardiac fibrosis
19 and restore cardiac function using an angiotensin II/phenylephrine-induced hypertensive heart failure
20 mouse model ¹².

21 Thus, FAP appears an attractive therapeutic target for fibrotic heart failure and atherosclerosis worth
22 being further investigated in the clinical arena.

1 **Funding**

2 This work was supported by the Swiss National Science Foundation (PZOO3_161521 to S.S. and
3 310030_165990 and 320030_189229 to C.M.M.), the Novartis Foundation for medical-biological
4 Research (#16B103 to S.S.), the Olga-Mayenfisch Foundation (to S.S.), the SwissLife Foundation (to
5 S.S.), and the OPO Foundation (to S.S.), the Swiss Heart Foundation (to S.N.-S., S.S. and C.M.M.),
6 and by Matching Funds UZH, University Research Priority Program Integrative Human Physiology at
7 the University of Zurich (to C.M.M.).

8

9 **Conflict of Interest**

10 None declared.

11

12 **Author Contributions**

- 13 • Christian Matter initiated the study.
- 14 • Sokrates Stein and Christian Matter designed the experiments and co-supervised the
15 study.
- 16 • Julien Weber, Stefanie Nusser-Stein, Jürgen Pahla, Shafeeq Mohammed, Sara Oppi,
17 Daniel S. Gaul, and Sokrates Stein performed experiments and data analyses.
- 18 • Hui E. Zhang and Mark D. Gorrell performed the SILAC-mass spec analysis.
- 19 • Ferdinand von Meyenn provided support with the scRNA-seq analyses.
- 20 • Anne Tailleux and Bart Staels performed lipoprotein analyses.
- 21 • Sokrates Stein, Christian Matter, and Mark D. Gorrell wrote the manuscript.
- 22 • Francesco Paneni, Frank Ruschitzka and Thomas F. Lüscher edited the manuscript.
- 23 • Christian Matter, Sokrates Stein, Frank Ruschitzka and Thomas F. Lüscher obtained
24 funding for the study.

25

26 **Data Availability Statement**

27 The data underlying this article is either publicly available (transcriptomic data) or will be shared on
28 reasonable request to the corresponding author.

29

1 **References**

- 2 1. Stary HC, Chandler AB, Dinsmore RE, Fuster V, Glagov S, Insull Jr W, Rosenfeld ME,
3 Schwartz CJ, Wagner WD, Wissler RW. A Definition of Advanced Types of Atherosclerotic
4 Lesions and a Histological Classification of Atherosclerosis. *Arterioscler Thromb Vasc Biol*
5 1995;15:12-1531.
- 6 2. Stary HC, Chandler AB, Glagov S, Guyton JR, Insull Jr W, Rosenfeld ME, Schaffer SA,
7 Schwartz CJ, Wagner WD, Wissler RW. A definition of initial, fatty streak, and intermediate
8 lesions of atherosclerosis. A report from the Committee on Vascular Lesions of the Council on
9 Arteriosclerosis, American Heart Association. *Arterioscler Thromb Vasc Biol* 1994;1994:840-
10 856.
- 11 3. Galis ZS, Sukhova GK, Lark MW, Libby P. Increased Expression of Matrix Metalloproteinases
12 and Matrix Degrading Activity in Vulnerable Regions of Human Atherosclerotic Plaques. *J*
13 *Clin Invest* 1994;94:2493-2503.
- 14 4. Libby P. Mechanisms of acute coronary syndromes and their implications for therapy. *The*
15 *New England journal of medicine* 2013;368:2004-2013.
- 16 5. Libby P, Kobold S. Inflammation: a common contributor to cancer, aging, and cardiovascular
17 diseases-expanding the concept of cardio-oncology. *Cardiovasc Res* 2019;115:824-829.
- 18 6. Park JE, Lenter MC, Zimmermann RN, Garin-Chesa P, Old LJ, Rettig WJ. Fibroblast
19 activation protein, a dual specificity serine protease expressed in reactive human tumor
20 stromal fibroblasts. *J Biol Chem* 1999;274:36505-36512.
- 21 7. Christiansen VJ, Jackson KW, Lee KN, McKee PA. Effect of fibroblast activation protein and
22 alpha2-antiplasmin cleaving enzyme on collagen types I, III, and IV. *Arch Biochem Biophys*
23 2007;457:177-186.

- 1 8. Zhang HE, Hamson EJ, Koczorowska MM, Tholen S, Chowdhury S, Bailey CG, Lay AJ,
2 Twigg SM, Lee Q, Roediger B, Biniossek ML, O'Rourke MB, McCaughan GW, Keane FM,
3 Schilling O, Gorrell MD. Identification of Novel Natural Substrates of Fibroblast Activation
4 Protein-alpha by Differential Degradomics and Proteomics. *Molecular & cellular proteomics* :
5 *MCP* 2019;**18**:65-85.
- 6 9. Bauer S, Jendro MC, Wadle A, Kleber S, Stenner F, Dinser R, Reich A, Faccin E, Godde S,
7 Dinges H, Muller-Ladner U, Renner C. Fibroblast activation protein is expressed by
8 rheumatoid myofibroblast-like synoviocytes. *Arthritis Res Ther* 2006;**8**:R171.
- 9 10. Edosada CY, Quan C, Wiesmann C, Tran T, Sutherlin D, Reynolds M, Elliott JM, Raab H,
10 Fairbrother W, Wolf BB. Selective inhibition of fibroblast activation protein protease based on
11 dipeptide substrate specificity. *J Biol Chem* 2006;**281**:7437-7444.
- 12 11. Keane FM, Yao TW, Seelk S, Gall MG, Chowdhury S, Poplawski SE, Lai JH, Li Y, Wu W,
13 Farrell P, Vieira de Ribeiro AJ, Osborne B, Yu DM, Seth D, Rahman K, Haber P, Topaloglu
14 AK, Wang C, Thomson S, Hennessy A, Prins J, Twigg SM, McLennan SV, McCaughan GW,
15 Bachovchin WW, Gorrell MD. Quantitation of fibroblast activation protein (FAP)-specific
16 protease activity in mouse, baboon and human fluids and organs. *FEBS Open Bio* 2013;**4**:43-
17 54.
- 18 12. Aghajanian H, Kimura T, Rurik JG, Hancock AS, Leibowitz MS, Li L, Scholler J, Monslow J,
19 Lo A, Han W, Wang T, Bedi K, Morley MP, Linares Saldana RA, Bolar NA, McDaid K,
20 Assenmacher CA, Smith CL, Wirth D, June CH, Margulies KB, Jain R, Pure E, Albelda SM,
21 Epstein JA. Targeting cardiac fibrosis with engineered T cells. *Nature* 2019;**573**:430-433.
- 22 13. Brokopp CE, Schoenauer R, Richards P, Bauer S, Lohmann C, Emmert MY, Weber B,
23 Winnik S, Aikawa E, Graves K, Genoni M, Vogt P, Luscher TF, Renner C, Hoerstrup SP,
24 Matter CM. Fibroblast activation protein is induced by inflammation and degrades type I
25 collagen in thin-cap fibroatheromata. *Eur Heart J* 2011;**32**:2713-2722

- 1 14. Tan SY, Chowdhury S, Polak N, Gorrell MD, Weninger W. Fibroblast activation protein is
2 dispensable in the anti-influenza immune response in mice. *PLoS One* 2017;**12**:e0171194.
- 3 15. Niedermeyer J, Kriz M, Hilberg F, Garin-Chesa P, Bamberger U, Lenter MC, Park J, Viertel B,
4 Puschner H, Mauz M, Rettig WJ, Schnapp A. Targeted disruption of mouse fibroblast
5 activation protein. *Mol Cell Biol* 2000;**20**:1089-1094.
- 6 16. Lee KN, Jackson KW, Christiansen VJ, Lee CS, Chun JG, McKee PA. Antiplasmin-cleaving
7 enzyme is a soluble form of fibroblast activation protein. *Blood* 2006;**107**:1397-1404.
- 8 17. Hagg S, Skogsberg J, Lundstrom J, Noori P, Nilsson R, Zhong H, Maleki S, Shang MM,
9 Brinne B, Bradshaw M, Bajic VB, Samnegard A, Silveira A, Kaplan LM, Gigante B, Leander
10 K, de Faire U, Rosfors S, Lockowandt U, Liska J, Konrad P, Takolander R, Franco-Cereceda
11 A, Schadt EE, Ivert T, Hamsten A, Tegner J, Bjorkegren J. Multi-organ expression profiling
12 uncovers a gene module in coronary artery disease involving transendothelial migration of
13 leukocytes and LIM domain binding 2: the Stockholm Atherosclerosis Gene Expression
14 (STAGE) study. *PLoS Genet* 2009;**5**:e1000754.
- 15 18. Oppi S, Nusser-Stein S, Blyszczuk P, Wang X, Jomard A, Marzolla V, Yang K, Velagapudi S,
16 Ward LJ, Yuan XM, Geiger MA, Guillaumon AT, Othman A, Hornemann T, Rancic Z, Ryu D,
17 Oosterveer MH, Osto E, Luscher TF, Stein S. Macrophage NCOR1 protects from
18 atherosclerosis by repressing a pro-atherogenic PPARgamma signature. *Eur Heart J*
19 2020;**41**:995-1005.
- 20 19. Gu W, Ni Z, Tan YQ, Deng J, Zhang SJ, Lv ZC, Wang XJ, Chen T, Zhang Z, Hu Y, Jing ZC,
21 Xu Q. Adventitial Cell Atlas of wt (Wild Type) and ApoE (Apolipoprotein E)-Deficient Mice
22 Defined by Single-Cell RNA Sequencing. *Arterioscler Thromb Vasc Biol* 2019;**39**:1055-1071.
- 23 20. Oppi S, Luscher TF, Stein S. Mouse Models for Atherosclerosis Research-Which Is My Line?
24 *Front Cardiovasc Med* 2019;**6**:46.

- 1 21. Santos AM, Jung J, Aziz N, Kissil JL, Pure E. Targeting fibroblast activation protein inhibits
2 tumor stromagenesis and growth in mice. *J Clin Invest* 2009;**119**:3613-3625.
- 3 22. Hutcheson JD, Goettsch C, Bertazzo S, Maldonado N, Ruiz JL, Goh W, Yabusaki K, Faits T,
4 Bouten C, Franck G, Quillard T, Libby P, Aikawa M, Weinbaum S, Aikawa E. Genesis and
5 growth of extracellular-vesicle-derived microcalcification in atherosclerotic plaques. *Nat Mater*
6 2016;**15**:335-343.
- 7 23. Cox G, Kable E, Jones A, Fraser I, Manconi F, Gorrell MD. 3-dimensional imaging of collagen
8 using second harmonic generation. *J Struct Biol* 2003;**141**:53-62.
- 9 24. Tabula Muris C, Overall c, Logistical c, Organ c, processing, Library p, sequencing,
10 Computational data a, Cell type a, Writing g, Supplemental text writing g, Principal i. Single-
11 cell transcriptomics of 20 mouse organs creates a Tabula Muris. *Nature* 2018;**562**:367-372.
- 12 25. Uitte de Willige S, Malfliet J, Abdul S, Leebeek FWG, Rijken DC. The level of circulating
13 fibroblast activation protein correlates with incorporation of alpha-2-antiplasmin into the fibrin
14 clot. *Thromb Res* 2018;**166**:19-21.
- 15 26. Uitte de Willige S, Malfliet JJ, Deckers JW, Dippel DW, Leebeek FW, Rijken DC. Plasma
16 levels of soluble fibroblast activation protein in arterial thrombosis: determinants and cleavage
17 of its substrate alpha-2-antiplasmin. *Int J Cardiol* 2015;**178**:105-110.
- 18 27. Tillmanns J, Widera C, Habbaba Y, Galuppo P, Kempf T, Wollert KC, Bauersachs J.
19 Circulating concentrations of fibroblast activation protein alpha in apparently healthy
20 individuals and patients with acute coronary syndrome as assessed by sandwich ELISA. *Int J*
21 *Cardiol* 2013;**168**:3926-3931.

- 1 28. Tillmanns J, Fraccarollo D, Galuppo P, Wollert KC, Bauersachs J. Changes in concentrations
2 of circulating fibroblast activation protein alpha are associated with myocardial damage in
3 patients with acute ST-elevation MI. *Int J Cardiol* 2017;**232**:155-159.
- 4 29. Baerts L, Brouns R, Kehoe K, Verkerk R, Engelborghs S, De Deyn PP, Hendriks D, De
5 Meester I. Acute Ischemic Stroke Severity, Progression, and Outcome Relate to Changes in
6 Dipeptidyl Peptidase IV and Fibroblast Activation Protein Activity. *Transl Stroke Res*
7 2017;**8**:157-164.
- 8 30. Lay AJ, Zhang HE, McCaughan GW, Gorrell MD. Fibroblast activation protein in liver fibrosis.
9 *Front Biosci (Landmark Ed)* 2019;**24**:1-17.
- 10 31. Arlien-Soborg MC, Grondahl C, Baek A, Dal J, Alle Madsen M, Hogild ML, Pedersen SB,
11 Bjerre M, Jorgensen JOL. Fibroblast activation protein is a GH target: A prospective study of
12 patients with acromegaly before and after treatment. *J Clin Endocrinol Metab* 2019.
- 13 32. Liu X, Wu H, Byrne M, Krane S, Jaenisch R. Type III collagen is crucial for collagen I
14 fibrillogenesis and for normal cardiovascular development. *Proc Natl Acad Sci U S A*
15 1997;**94**:1852-1856.
- 16 33. D'Hondt S, Guillemin B, Syx D, Symoens S, De Rycke R, Vanhoutte L, Toussaint W,
17 Lambrecht BN, De Paepe A, Keene DR, Ishikawa Y, Bachinger HP, Janssens S, Bertrand
18 MJM, Malfait F. Type III collagen affects dermal and vascular collagen fibrillogenesis and
19 tissue integrity in a mutant Col3a1 transgenic mouse model. *Matrix Biol* 2018;**70**:72-83.
- 20 34. Mao JR, Bristow J. The Ehlers-Danlos syndrome: on beyond collagens. *J Clin Invest*
21 2001;**107**:1063-1069.
- 22 35. Schwarze U, Schievink WI, Petty E, Jaff MR, Babovic-Vuksanovic D, Cherry KJ, Pepin M,
23 Byers PH. Haploinsufficiency for one COL3A1 allele of type III procollagen results in a

1 phenotype similar to the vascular form of Ehlers-Danlos syndrome, Ehlers-Danlos syndrome
2 type IV. *Am J Hum Genet* 2001;**69**:989-1001.

3 36. Smith LB, Hadoke PW, Dyer E, Denvir MA, Brownstein D, Miller E, Nelson N, Wells S,
4 Cheeseman M, Greenfield A. Haploinsufficiency of the murine Col3a1 locus causes aortic
5 dissection: a novel model of the vascular type of Ehlers-Danlos syndrome. *Cardiovasc Res*
6 2011;**90**:182-190.

7 37. Busek P, Mateu R, Zubal M, Kotackova L, Sedo A. Targeting fibroblast activation protein in
8 cancer - Prospects and caveats. *Front Biosci (Landmark Ed)* 2018;**23**:1933-1968.

9

Figures legends

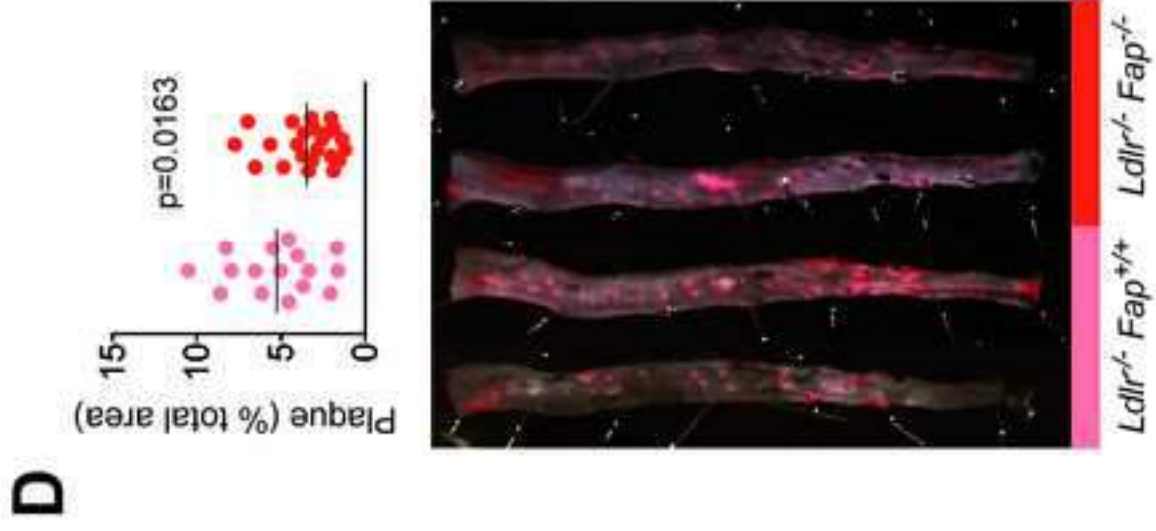
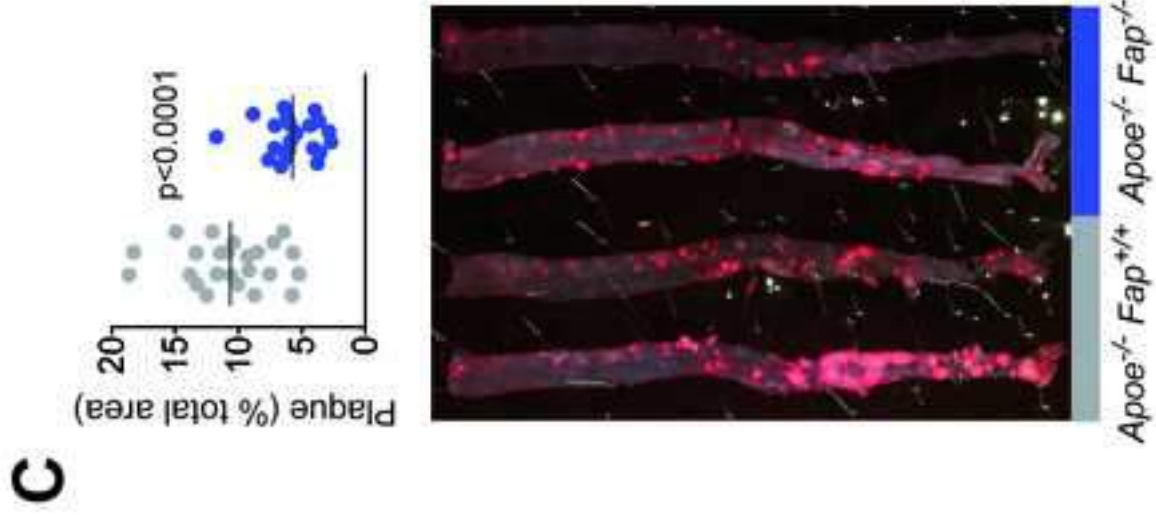
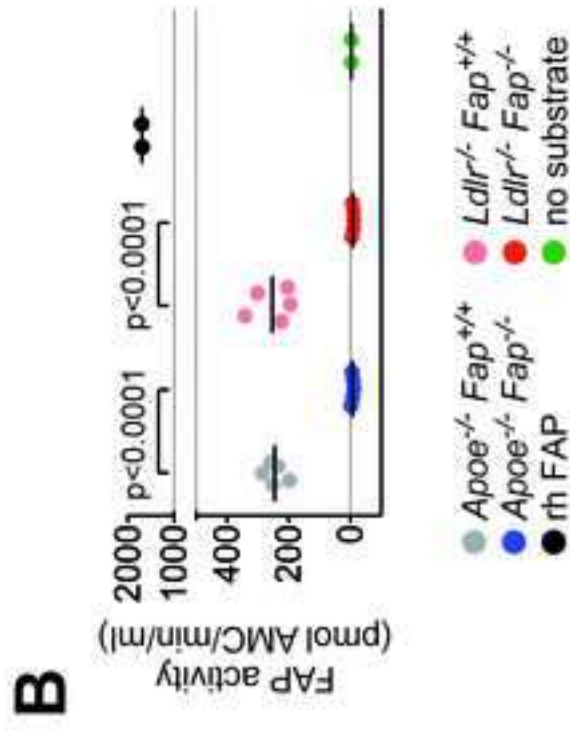
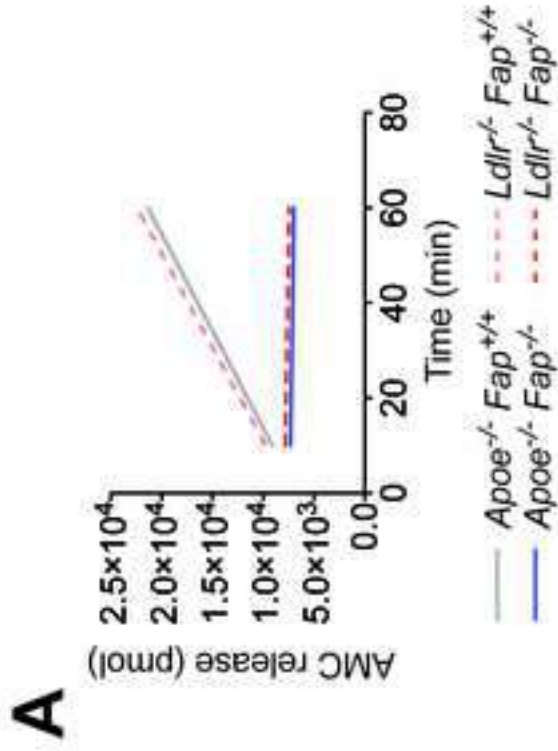
Figure 1. Constitutive *Fap* deletion reduces atherosclerosis development in mice. (A, B) FAP activity assay performed with plasma obtained from indicated mouse lines. (A) FAP activity as assessed by the FAP target 3144-aminomethylcoumarin (AMC) release curve. (B) Quantification of the AMC release over time. $n = 5$ per genotype, $n = 2$ for controls. rhFAP, recombinant human FAP. (C, D) Quantification and representative images of atherosclerotic lesions in thoraco-abdominal aortae stained with Oil-red O in the indicated genotypes. $n \geq 16$ per genotype. Scatter blots with means. (Adjusted) P values are indicated in the figures (99.9% confidence interval). Unpaired two-tailed Student's *t*-test (C, D); ANOVA analysis and Bonferroni post-hoc test (B).

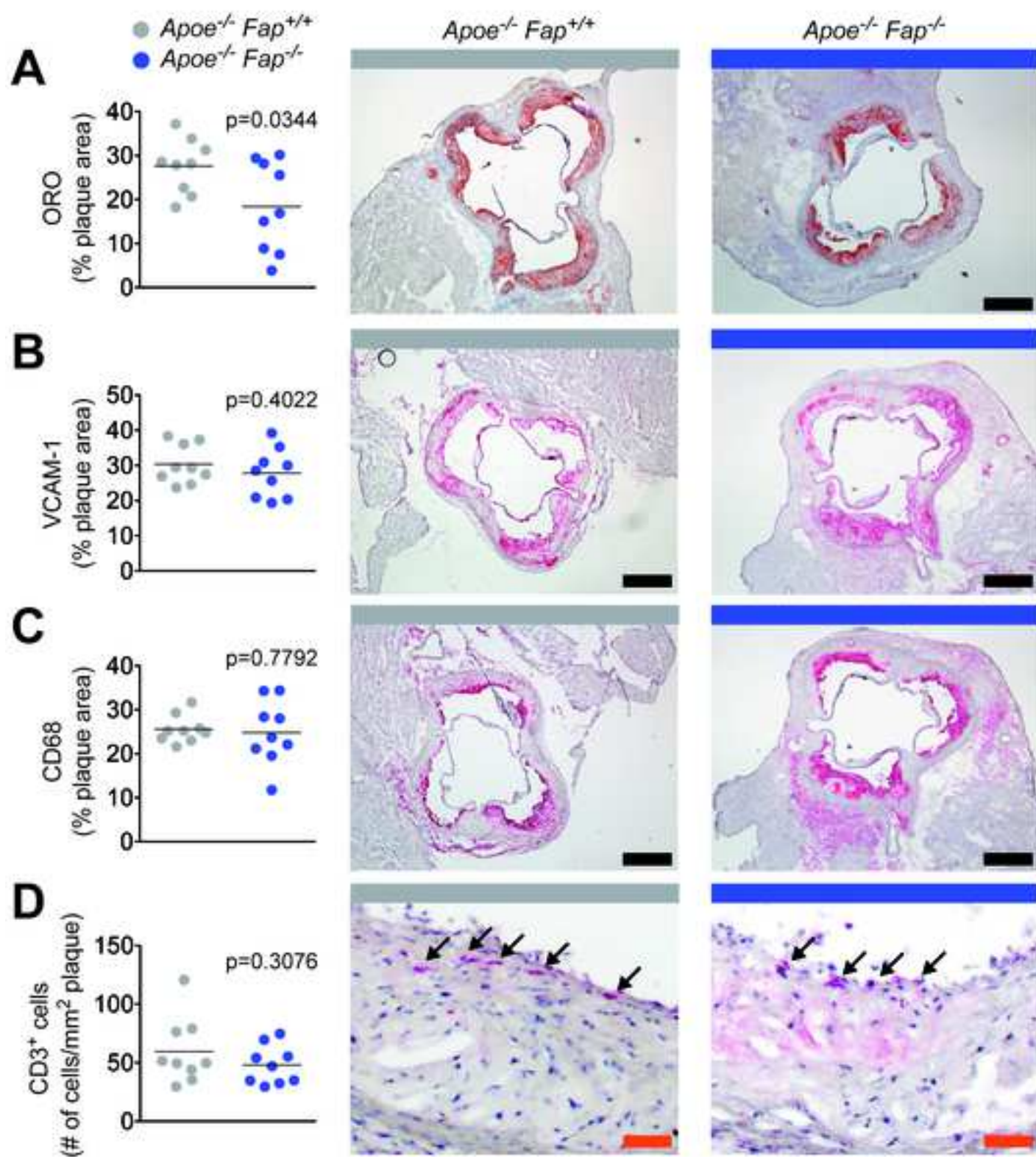
Figure 2. *Fap* deficiency diminishes accumulation of neutral lipids in atherosclerotic plaques of *Apoe*^{-/-} mice without affecting macrophages and T cells. (A) Quantification of neutral lipids and representative images of aortic sinus cross-sections with Oil-red O. (B-D) Quantification of immunohistochemical stainings and representative images of VCAM-1 (B), CD68 (C), and CD3 (D) in cross-sections from the aortic sinus. $n \geq 8$ per genotype (4 cross-sections per mouse). Black bars = 400 μm , orange bars = 40 μm . Black arrows, examples of CD3-positive cells. Scatter blots with means, unpaired two-tailed Student's *t*-test.

Figure 3. *Fap* deletion alters collagen structure in atherosclerotic lesions. (A-D) Quantification of total collagen content (A), necrotic core size (B), fibrous cap thickness (C), and (D) representative images of aortic sinus cross-sections stained with Elastica van Gieson (EvG). Green line, fibrous cap; dashed green line, necrotic core. $n = 7$ *Apoe*^{-/-} *Fap*^{+/+} mice, $n = 9$ *Apoe*^{-/-} *Fap*^{-/-}. (E) Quantification of collagen content and representative images of aortic sinus cross-sections stained with Sirius Red and visualized under normal light. $n = 7$ *Apoe*^{-/-} *Fap*^{+/+} mice, $n = 9$ *Apoe*^{-/-} *Fap*^{-/-}. (F) Representative images of second harmonics generation (SHG) and quantification of fibrillar collagen in aortic sinus cross-sections. $n = 9$ *Apoe*^{-/-} *Fap*^{+/+} mice, $n = 6$ *Apoe*^{-/-} *Fap*^{-/-}. Black and white bars = 400 μm , orange bars = 100 μm . Scatter blots with means, unpaired two-tailed Student's *t*-test (A-E); nonparametric Mann-Whitney test (F).

Figure 4. Cleavage events in collagens revealed by proteomics in the secretomes of mouse embryonic fibroblasts that express active FAP compared with inactive FAP. (A-D) Log transformed fold-change of neo-N-terminal peptides is shown for individual cleavage sites and arranged by amino acid position for COL1A1 (A), COL1A2 (B), COL3A1 (C), and COL5A2 (D). Neo-N-terminal peptides resulting from cleavage after Gly-Pro are represented by coloured squares, whereas other cleavage sites are plotted as black circles. A fold change ≥ 0.58 represents increased peptide abundance of $\geq 50\%$ in the presence of FAP activity. A fold change ≤ -0.58 represents decreased peptide abundance of $\geq 50\%$ in the presence of FAP activity. Mean and standard deviation of data that reached significance (limma statistic with $p < 0.05$). (E, F) COL3A1 immunoblots from aortae from *Apoe*^{-/-} *Fap*^{-/-} and *Apoe*^{-/-} *Fap*^{+/+} mice. Pre, precursor COL3A1; cleaved, cleaved COL3A1 fibers. $n = 4$ per genotype. (G) Expression of *FAP* in biopsies of non-atherosclerotic mammary arteries (Mammary) and atherosclerotic aortic roots (Athero) (raw data, GSE40231). Unpaired two-tailed Student's *t*-test (F, G).

Figure 5. Graphical abstract. Scheme demonstrating how the deletion of FAP protects against atherosclerosis development.





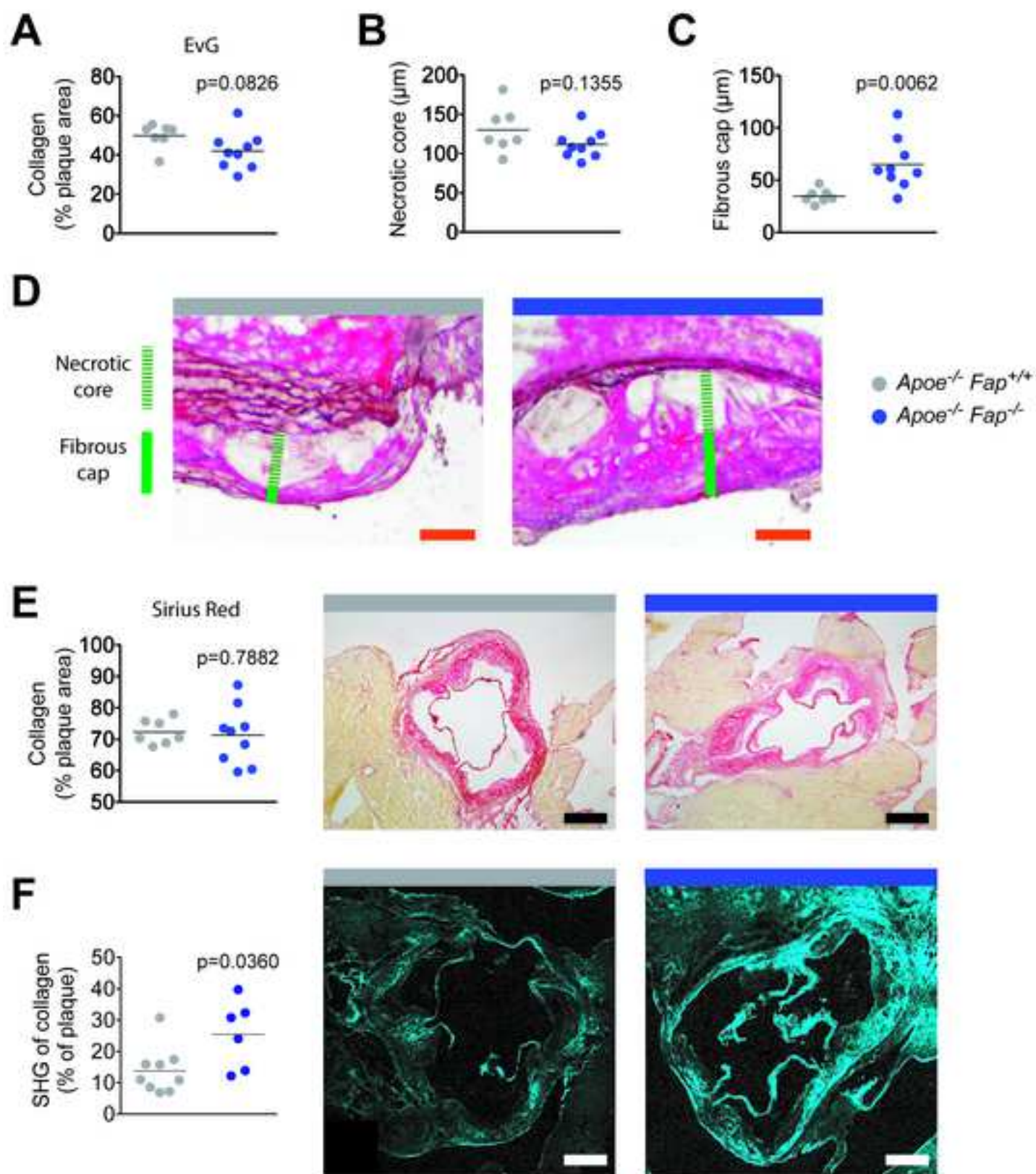
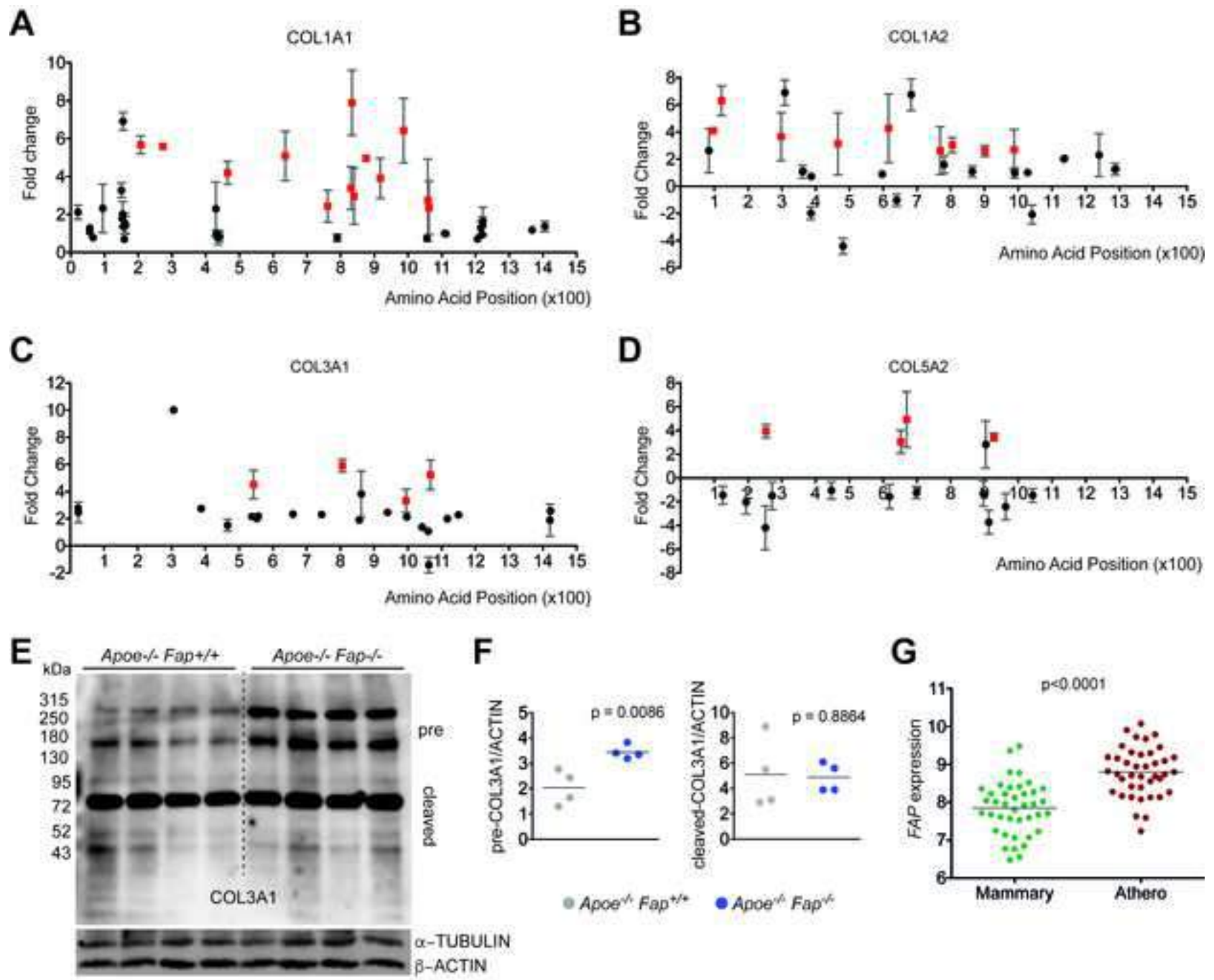
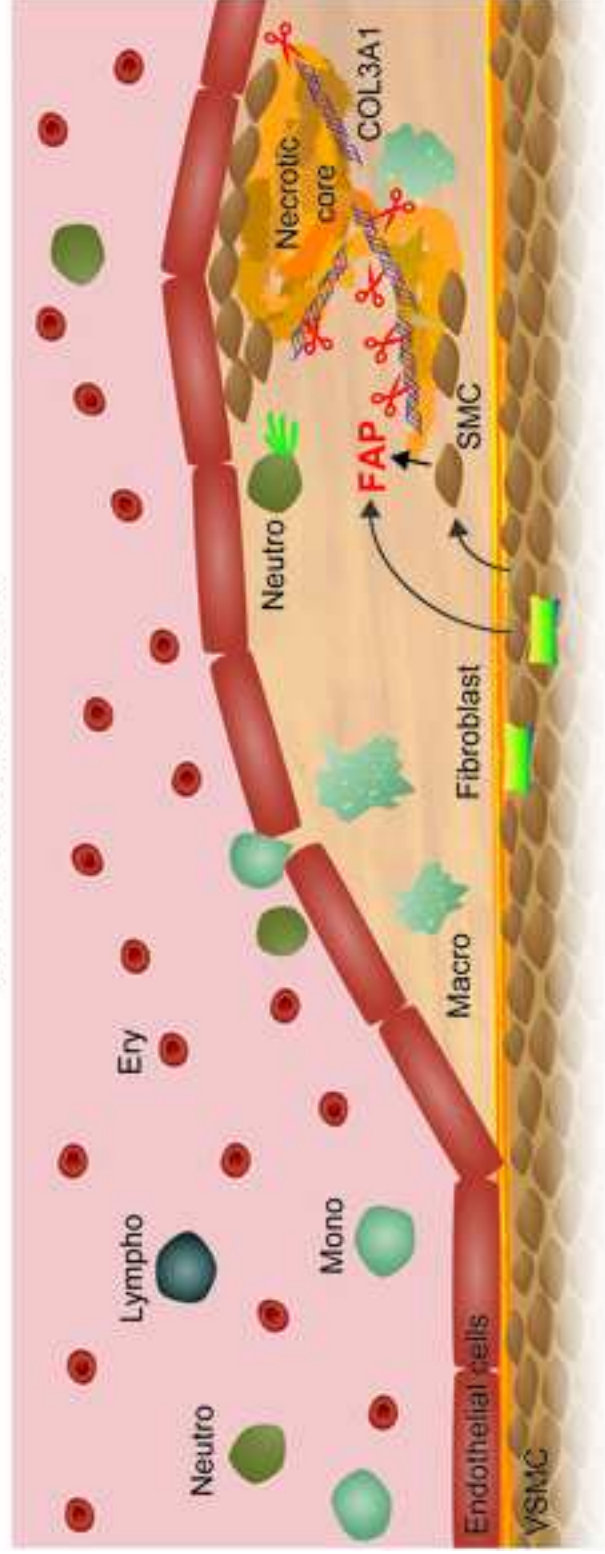


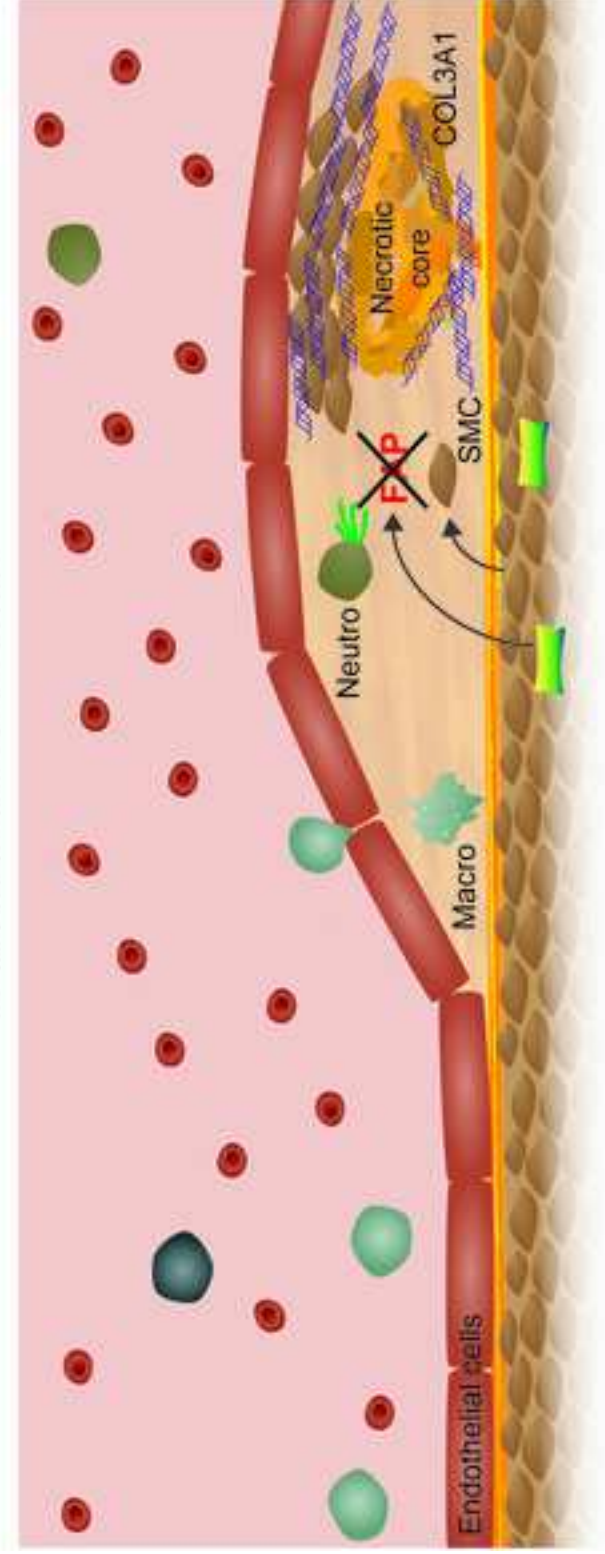
Figure 4



Normal endogenous FAP

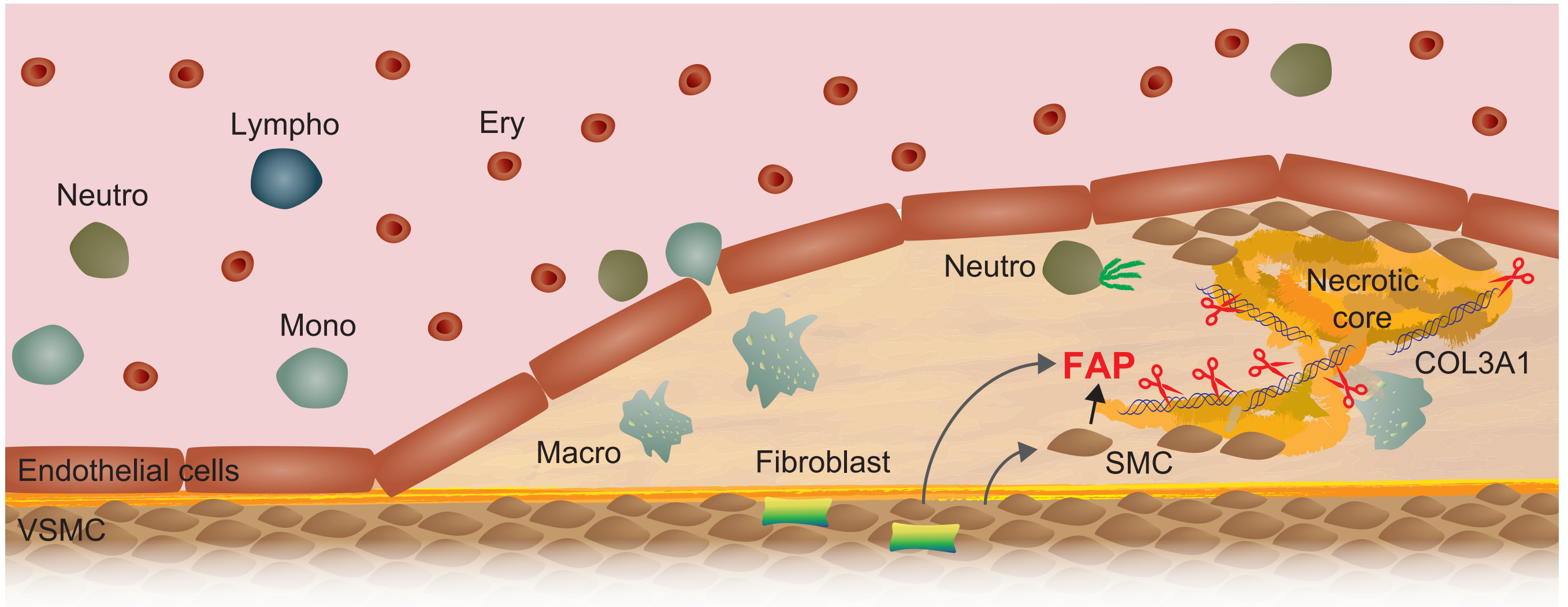


Constitutive FAP deletion

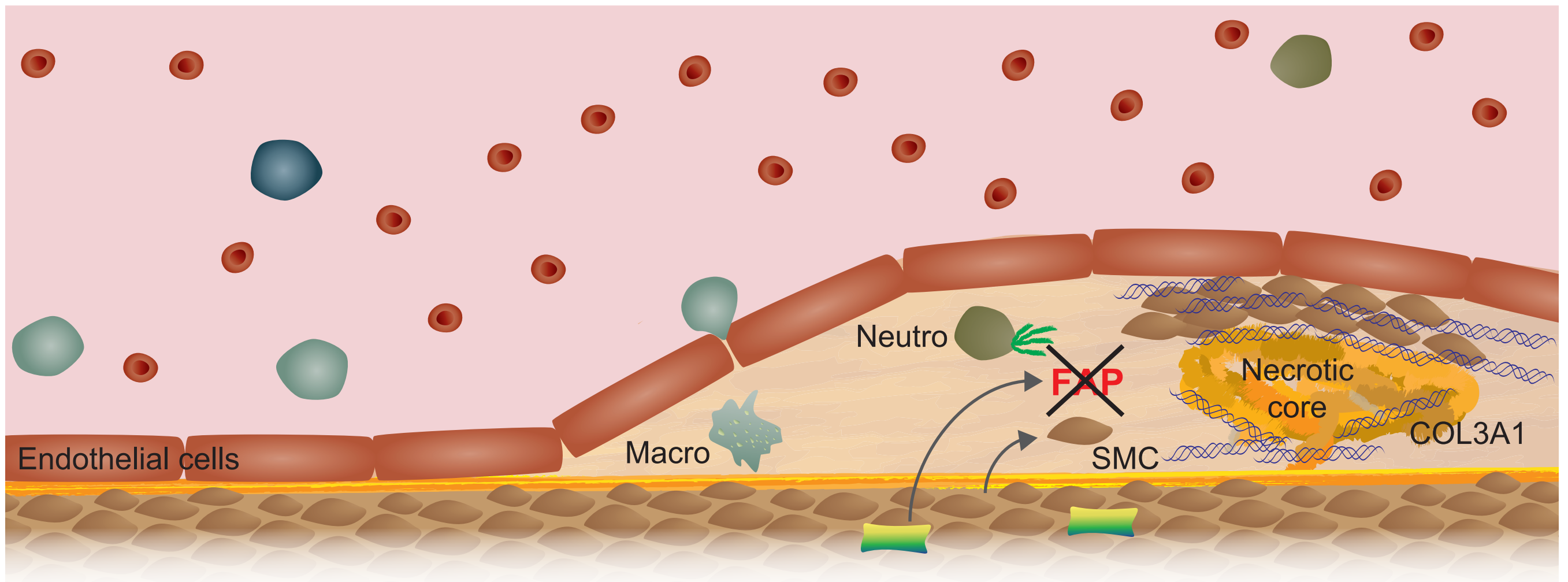


More pre-COL3A1, thicker fibrous caps, and less atherosclerotic lesions

Normal endogenous FAP



Constitutive FAP deletion



More pre-COL3A1, thicker fibrous caps, and less atherosclerotic lesions

Supplemental Information for

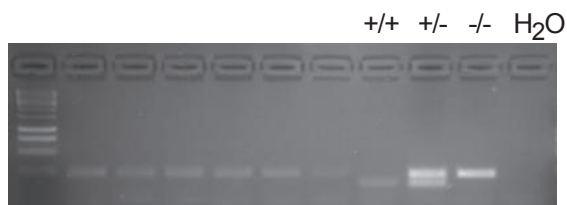
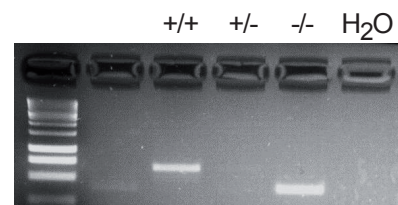
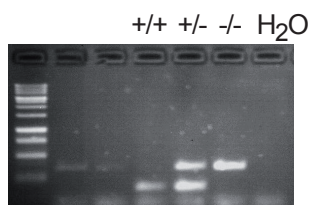
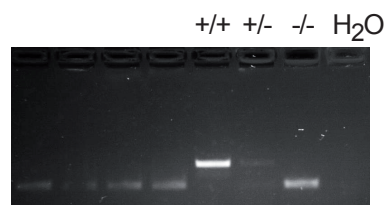
Deletion of fibroblast activation protein provides atheroprotectionContact e-mail: sokrates.stein@uzh.ch and christian.matter@usz.ch**Figure S1****A** *Apoe*^{-/-} *Fap*^{-/-} mice*Apoe* primers:*Fap* primers:**B** *Ldlr*^{-/-} *Fap*^{-/-} mice*Ldlr* primers:*Fap* primers:

Figure S1. Validation of the genotype of *Apoe*^{-/-} *Fap*^{-/-} and *Ldlr*^{-/-} *Fap*^{-/-} mice and the corresponding controls. (A, B) PCR validation of (A) *Apoe*^{-/-} *Fap*^{+/+} and *Apoe*^{-/-} *Fap*^{-/-} mice and (B) *Ldlr*^{-/-} *Fap*^{+/+} and *Ldlr*^{-/-} *Fap*^{-/-} mice.

Figure S2

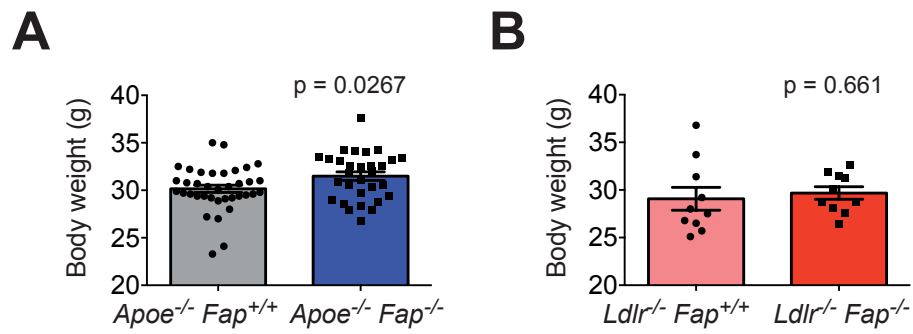


Figure S2. Body weight of atherosclerotic mice lacking *Fap*. **(A, B)** Body weight of **(A)** *Apoe*^{-/-} *Fap*^{+/+} and *Apoe*^{-/-} *Fap*^{-/-} mice and **(B)** *Ldlr*^{-/-} *Fap*^{+/+} and *Ldlr*^{-/-} *Fap*^{-/-} mice that were fed a high-cholesterol diet for 12 weeks. Data are represented in scatter plots and bars \pm standard error; unpaired two-tailed Student's *t*-test.

Figure S3

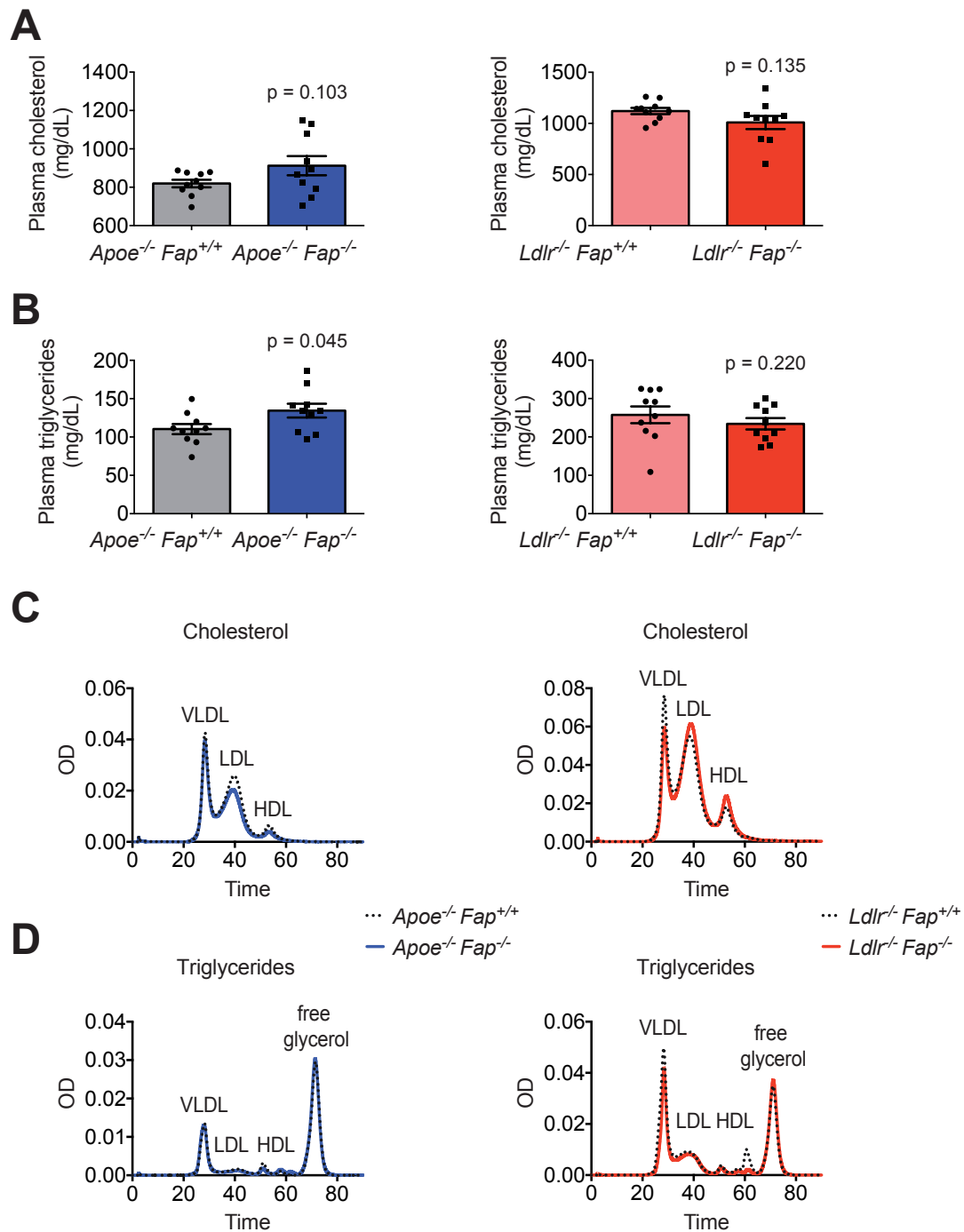


Figure S3. Plasma lipid levels in atherosclerotic *Fap*-deficient mice. **(A, B)** Total plasma cholesterol and **(B)** triglyceride levels in *Apoe*^{-/-} *Fap*^{+/+} versus *Apoe*^{-/-} *Fap*^{-/-} mice as well as in *Ldlr*^{-/-} *Fap*^{+/+} and *Ldlr*^{-/-} *Fap*^{-/-} mice. $n = 10$ per genotype. **(C, D)** Cholesterol and **(B)** triglycerides levels in lipoprotein subfractions of *Apoe*^{-/-} *Fap*^{+/+} versus *Apoe*^{-/-} *Fap*^{-/-} mice as well as in *Ldlr*^{-/-} *Fap*^{+/+} and *Ldlr*^{-/-} *Fap*^{-/-} mice. $n = 1$ pool from 10 mice per genotype. Data are represented in scatter plots and bars \pm standard error (A and B) or plotting individual values on a XY graph. unpaired two-tailed Student's *t*-test **(A, B)**.

Figure S4

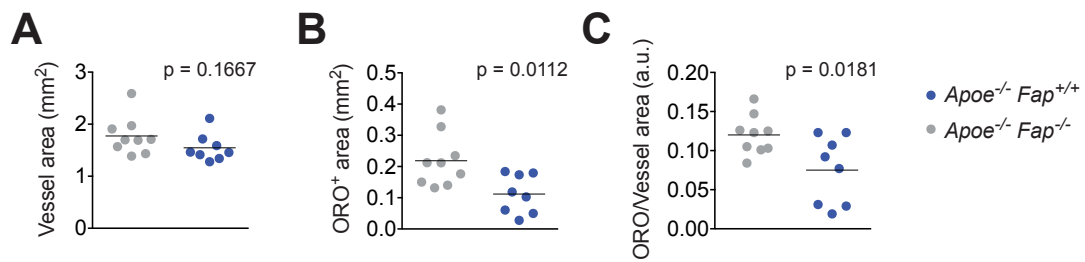


Figure S4. Aortic sinus plaque analysis. (A) Entire aortic sinus from *Apoe*^{-/-} *Fap*^{+/+} versus *Apoe*^{-/-} *Fap*^{-/-} mice. (B) Oil-red O-positive area in aortic sinus of *Apoe*^{-/-} *Fap*^{+/+} versus *Apoe*^{-/-} *Fap*^{-/-} mice. (C) Oil-red O-positive area relative to vessel area in aortic sinus of *Apoe*^{-/-} *Fap*^{+/+} versus *Apoe*^{-/-} *Fap*^{-/-} mice. n = 9 *Apoe*^{-/-} *Fap*^{+/+}, n = 8 *Apoe*^{-/-} *Fap*^{-/-} mice. Data are represented in scatter plots with means; unpaired two-tailed Student's *t*-test.

Figure S5

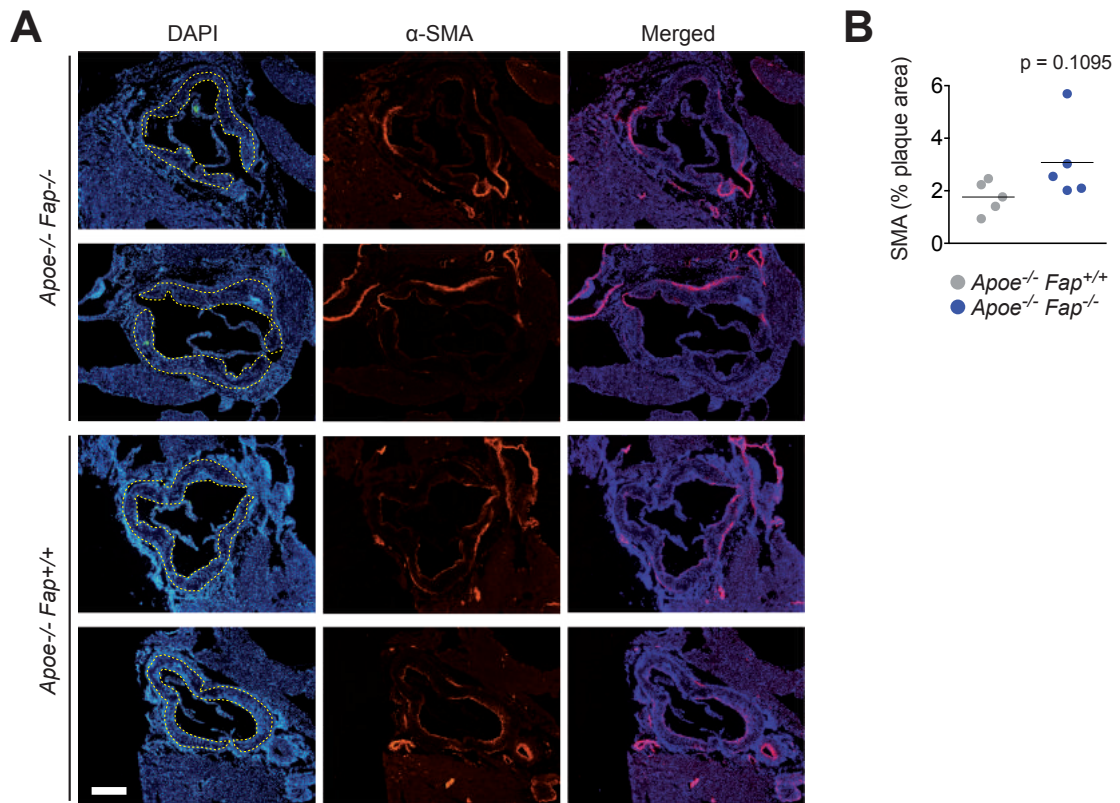


Figure S5. *Vascular smooth muscle cell staining.* (A, B) Representative images (A) and quantification (B) of intra-plaque α -smooth muscle actin (α -SMA) staining in cross-sections from the aortic sinus. The plaque area is marked in yellow dotted lines in the DAPI images. $n \geq 5$ per genotype (4 cross-sections per mouse). White bar = 400 μ m. Data are represented in scatter plots with means; unpaired two-tailed Student's *t*-test.

Figure S6

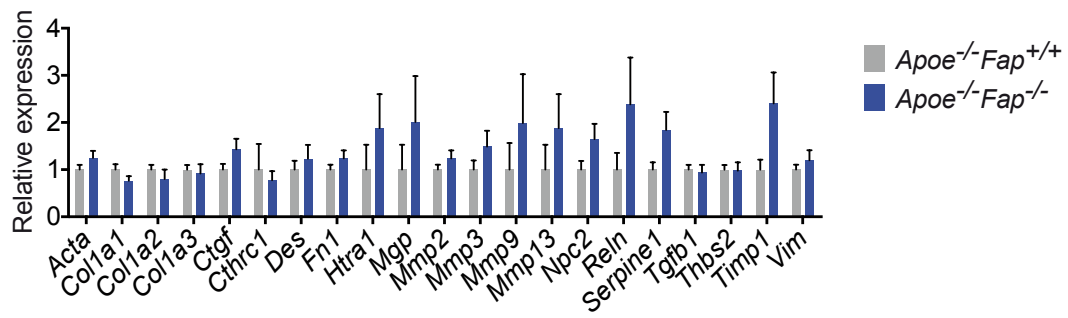


Figure S6. Expression levels of extracellular matrix modulators. mRNA expression of collagens, matrix metalloproteinases, and markers of fibrosis in aortae from *Apoe*^{-/-} *Fap*^{+/+} versus *Apoe*^{-/-} *Fap*^{-/-} mice. n = 6 per genotype. Data are represented in bar graphs with means and standard errors.

Figure S7

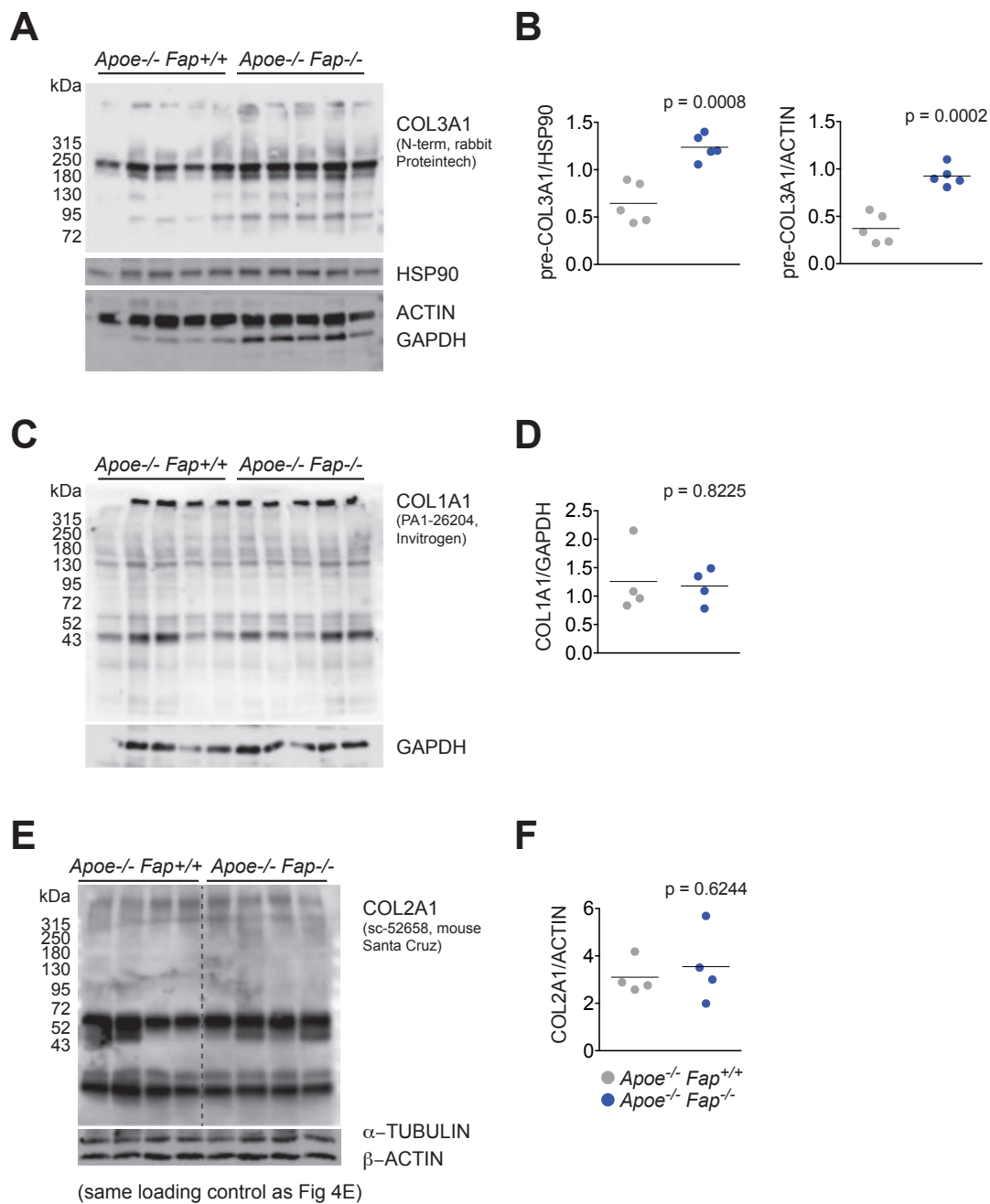


Figure S7. *COL13A1*, *COL1A1* and *COL2A1* protein levels in atherosclerotic *Fap*-deficient mice. (**A**, **B**) *COL3A1* immunoblots (**A**) from aortae from *Apoe*^{-/-} *Fap*^{-/-} and *Apoe*^{-/-} *Fap*^{+/+} mice and their quantification (**B**). n = 5 per genotype (**C**, **D**) *COL1A1* immunoblots (**C**) from aortae from *Apoe*^{-/-} *Fap*^{-/-} and *Apoe*^{-/-} *Fap*^{+/+} mice, respectively. n = 5 per genotype. (**D**) Quantification of *COL1A1* expression (n = 4 per genotype; the two external lanes were excluded). (**E**, **F**) *COL2A1* immunoblots (**E**) from aortae from *Apoe*^{-/-} *Fap*^{-/-} and *Apoe*^{-/-} *Fap*^{+/+} mice and their quantification (**F**). n = 4 per genotype. Data are represented in scatter plots with means; unpaired two-tailed Student's *t*-test.

Figure S8

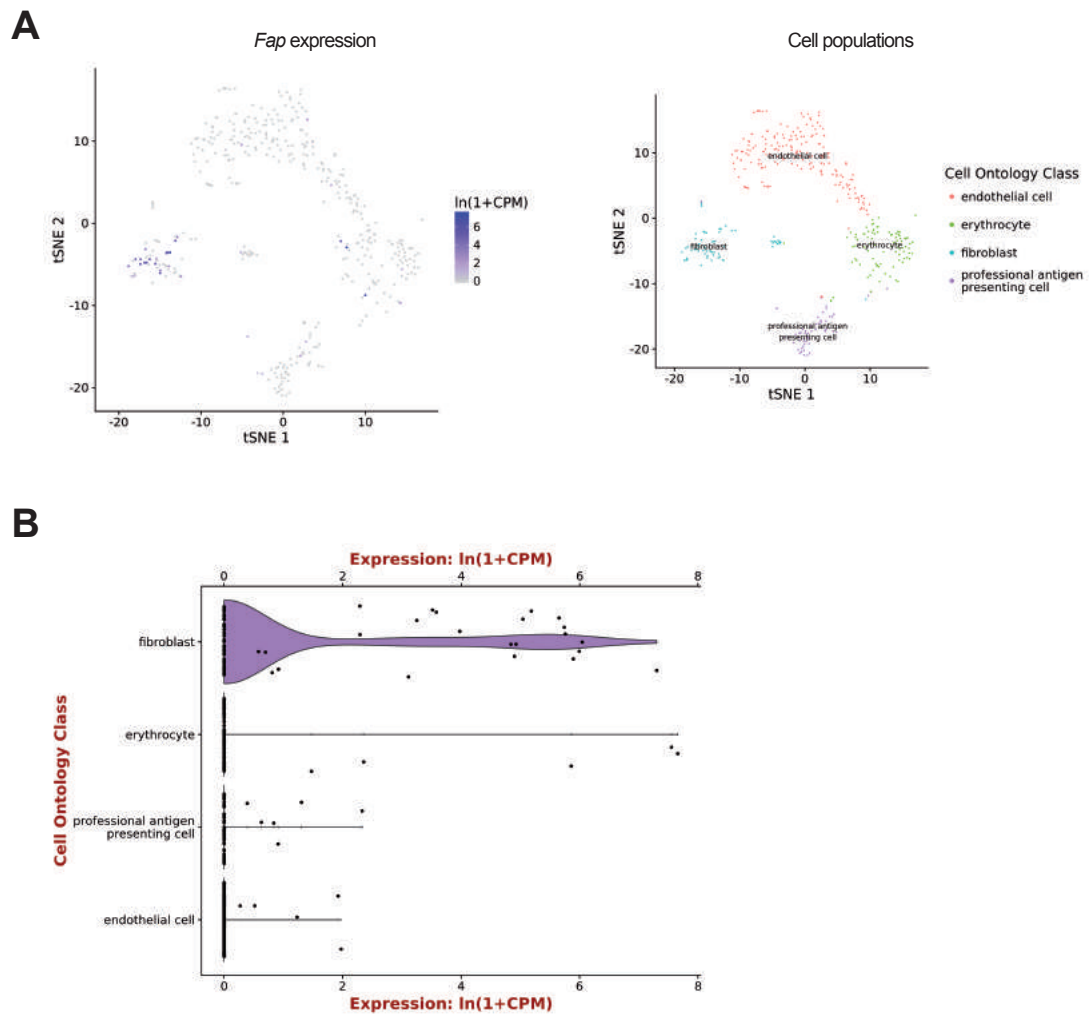


Figure S8. *Fap* expression in aortae of 3-month-old C57BL/6JN mice. **(A)** *Fap* expression in different aortic cell populations as described on the right panel. **(B)** Quantification of *Fap* expression in corresponding vascular cells. Graphs were directly exported from the *Tabula muris* dataset²⁴.

Table S1. Hematological analyses.

	WBC	RBC	PLT	Neutrophils		Lymphocytes		Monocytes		Eosinophils		Basophils	
	number 10 ⁹ /L	number 10 ¹² /L	number 10 ³ /μL	%	number 10 ³ /μL	%	number 10 ³ /μL	%	number 10 ³ /μL	%	number 10 ³ /μL	%	number 10 ³ /μL
<i>ApoE</i> ^{-/-} <i>Fap</i> ^{+/+} (n=10)	6.593 ± 0.5620	9.190 ± 0.1246	1891 ± 164.2	52.20 ± 2.401	3.502 ± 0.4123	39.18 ± 2.422	2.549 ± 0.2428	1.290 ± 0.2442	0.0790 ± 0.01130	2.790 ± 1.143	0.1630 ± 0.05727	0.4000 ± 0.06325	0.0260 ± 0.003712
<i>ApoE</i> ^{-/-} <i>Fap</i> ^{-/-} (n=12)	6.234 ± 0.7441	9.234 ± 0.2201	1480 ± 118.2	28.86 ± 1.881	1.694 ± 0.1213	61.47 ± 1.883	3.926 ± 0.6243	2.833 ± 0.2076	0.1767 ± 0.0255	3.700 ± 0.6370	0.2275 ± 0.04432	0.3750 ± 0.02787	0.02333 ± 0.002562
P value	0.7138	0.8704	0.0511	< 0.0001	0.0002	< 0.0001	0.0707	< 0.0001	0.0038	0.4760	0.3764	0.7051	0.5508
<i>Ldlr</i> ^{-/-} <i>Fap</i> ^{+/+} (n=9)	7.557 ± 0.9580	9.794 ± 0.1407	1208 ± 104.4	17.09 ± 1.656	1.199 ± 0.1184	74.19 ± 1.708	5.714 ± 0.8037	2.711 ± 0.4118	0.1967 ± 0.02867	2.422 ± 0.3800	0.1911 ± 0.03642	0.4667 ± 0.03333	0.03444 ± 0.005031
<i>Ldlr</i> ^{-/-} <i>Fap</i> ^{-/-} (n=10)	9.163 ± 0.4785	9.808 ± 0.09269	1414 ± 140.5	13.50 ± 0.7397	1.241 ± 0.09821	79.31 ± 1.316	7.252 ± 0.3676	2.750 ± 0.4342	0.2560 ± 0.04190	1.580 ± 0.4685	0.1442 ± 0.05537	0.4500 ± 0.03727	0.0420 ± 0.005121
P value	0.14	0.9356	0.2644	0.056	0.786	0.028	0.0894	0.9492	0.2691	0.1866	0.499	0.7452	0.3091

WBC, white blood cell; PLT, platelets; RBC, red blood cells; unpaired two-tailed Student's *t*-test.

Table S2. Selection of the highest transcripts in cells expressing *Fap* in atherosclerotic *Apoe* aortae.

CATCCAC AGATCCT GT-1	CCTACAC TCCAATG GT-1	GTATTCT CATGCTA GT-1	GTGCATA GTATCGC AT-1	CACACTC GTTTAGG AA-1	CCTTCGA TCCACTC CA-1	CTTGGCT GTCAAGC GA-1	GACGCGT GTATCTG CA-1	GCTCTGT AGCGTCA AG-1	GGACAAG GTAAATA CG-1	TGCCCTA CAAGCCG TC-1	TGGCGCA CAAGGAC TG-1	TGTGGTA AGGCGAC AT-1
<i>Col3a1</i>	<i>Dcn</i>	<i>Mgp</i>	<i>Gsn</i>	<i>Gsn</i>	<i>Dcn</i>	<i>Gsn</i>	<i>Gsn</i>	<i>Cyt11</i>	<i>Gsn</i>	<i>Dcn</i>	<i>Dcn</i>	<i>Gsn</i>
<i>S100a6</i>	<i>Gsn</i>	<i>Cst3</i>	<i>Dcn</i>	<i>S100a6</i>	<i>Gsn</i>	<i>Dcn</i>	<i>S100a6</i>	<i>Cst3</i>	<i>Dcn</i>	<i>Tmsb4x</i>	<i>Tmsb4x</i>	<i>Dcn</i>
<i>Tmsb4x</i>	<i>Rps27</i>	<i>Dcn</i>	<i>Tmsb4x</i>	<i>Dcn</i>	<i>Ftl1</i>	<i>Tmsb4x</i>	<i>Dcn</i>	<i>Rpl41</i>	<i>Mgp</i>	<i>Rpl41</i>	<i>Rpl41</i>	<i>Mfap5</i>
<i>Col1a2</i>	<i>Rpl41</i>	<i>Igfbp7</i>	<i>Rpl41</i>	<i>Ftl1</i>	<i>S100a6</i>	<i>B2m</i>	<i>Ftl1</i>	<i>Gsn</i> <i>31100790</i>	<i>Igfbp7</i>	<i>S100a6</i>	<i>Gsn</i>	<i>S100a6</i>
<i>Fn1</i>	<i>Mfap5</i>	<i>Lum</i>	<i>Mfap5</i>	<i>Tmsb4x</i>	<i>Ifitm3</i>	<i>Ftl1</i>	<i>Cst3</i>	<i>15Rik</i>	<i>Mt1</i>	<i>Mfap5</i>	<i>Ftl1</i>	<i>Rpl41</i>
<i>Dcn</i>	<i>Rps19</i>	<i>Rpl41</i>	<i>Rps27</i>	<i>Rpl41</i>	<i>Rpl41</i>	<i>S100a6</i>	<i>Col3a1</i>	<i>Mia</i>	<i>Ftl1</i>	<i>Col1a2</i>	<i>Cxcl1</i>	<i>Mt1</i>
<i>Mfap5</i>	<i>Ftl1</i>	<i>Cfh</i>	<i>Rpl37a</i>	<i>Mt1</i>	<i>B2m</i>	<i>Rpl41</i>	<i>Rpl41</i>	<i>Rps19</i>	<i>Rpl41</i>	<i>Rpl35</i>	<i>S100a6</i>	<i>Igfbp5</i>
<i>Postn</i>	<i>Rpl37a</i>	<i>Ftl1</i>	<i>Ftl1</i>	<i>Fn1</i>	<i>Penk</i>	<i>Ifitm3</i>	<i>Tmsb4x</i>	<i>Rpl37a</i>	<i>Hbb-bs</i>	<i>Ftl1</i>	<i>Rps27</i>	<i>Mt2</i>
<i>Rpl41</i>	<i>Rps3a1</i>	<i>Gsn</i>	<i>S100a6</i>	<i>Rpl35</i>	<i>Mt2</i>	<i>Tnfaip6</i>	<i>Rpl37a</i>	<i>Rps6</i>	<i>B2m</i>	<i>Tmsb10</i>	<i>Mt1</i>	<i>Tmsb4x</i>
<i>Serpinh1</i>	<i>Rpl35</i>	<i>Tmsb4x</i>	<i>Rpl35</i>	<i>Rps19</i>	<i>Tmsb4x</i>	<i>Rps27</i>	<i>B2m</i>	<i>Rps5</i>	<i>Ifitm3</i>	<i>Gsn</i>	<i>Rpl37a</i>	<i>Rps27</i>
<i>Gsn</i>	<i>Rpl32</i>	<i>Bgn</i>	<i>Rps19</i>	<i>Rpl37a</i>	<i>Rarres2</i>	<i>Rpl10</i>	<i>Igfbp7</i>	<i>Rps4x</i>	<i>Tmsb4x</i>	<i>Rps19</i>	<i>Rps19</i>	<i>Hbb-bs</i>
<i>Vim</i>	<i>S100a6</i>	<i>Hbb-bs</i>	<i>Rpl18a</i>	<i>Ubc</i>	<i>Rps27</i>	<i>Cxcl1</i>	<i>Rpl32</i>	<i>Rpl35</i>	<i>Rpl37a</i>	<i>Col3a1</i>	<i>Rps4x</i>	<i>Ftl1</i>
<i>S100a10</i>	<i>Hbb-bs</i>	<i>Rps27</i>	<i>Rpl10</i>	<i>Vim</i>	<i>Pcolce</i>	<i>Rpl37a</i>	<i>Hbb-bs</i>	<i>Rps11</i>	<i>Bgn</i>	<i>Mt2</i>	<i>Rps5</i>	<i>Rpl35</i>
<i>Ftl1</i>	<i>Rpl10</i>	<i>Rpl37a</i>	<i>Rps8</i>	<i>Rps27</i>	<i>Col1a2</i>	<i>S100a9</i>	<i>Ifitm2</i>	<i>Wif1</i>	<i>Jund</i>	<i>Rpl37a</i>	<i>Mfap5</i>	<i>S100a8</i>
<i>Serf2</i>	<i>Serping1</i>	<i>Vim</i>	<i>Igfbp5</i>	<i>Rpl18a</i>	<i>Lum</i>	<i>Rps19</i>	<i>Rps27</i>	<i>Rplp0</i>	<i>Junb</i>	<i>Rps27</i>	<i>Cst3</i>	<i>S100a11</i>
<i>Tppp3</i>	<i>Rps8</i>	<i>Rps5</i>	<i>Rps15a</i>	<i>Rps5</i>	<i>Plac8</i>	<i>Tmsb10</i>	<i>Ifitm3</i>	<i>Rpl18a</i>	<i>Mt2</i>	<i>S100a11</i>	<i>Rpl18a</i>	<i>Rpl18a</i>
<i>Cxcl2</i>	<i>Mt2</i>	<i>Rplp0</i>	<i>Vim</i>	<i>Dpt</i>	<i>Tmsb10</i>	<i>Rpl35</i>	<i>Rpl35</i>	<i>Vim</i>	<i>Rps27</i>	<i>Rpl18a</i>	<i>Rpl10</i>	<i>Tmsb10</i>
<i>Cd63</i>	<i>Rps9</i>	<i>Rpl13a</i>	<i>Rpl32</i>	<i>Rpl32</i>	<i>S100a9</i>	<i>Hbb-bs</i>	<i>Rpl10</i>	<i>Rps27</i>	<i>Rps19</i>	<i>Rpl10</i>	<i>Vim</i>	<i>Rpl37a</i>
<i>Hbb-bs</i>	<i>Rpl18a</i>	<i>S100a8</i>	<i>Rpl9</i>	<i>Pcolce</i>	<i>Rps4x</i>	<i>Rpl13a</i>	<i>Rps4x</i>	<i>Rpl13a</i>	<i>Cst3</i>	<i>Igfbp5</i>	<i>Rps8</i>	<i>Rps19</i>
<i>Cxcl1</i>	<i>B2m</i>	<i>Cyt11</i>	<i>Rps3</i>	<i>Tppp3</i>	<i>Gstm1</i>	<i>Serpinh1</i>	<i>Col6a2</i>	<i>Rpl32</i>	<i>S100a6</i>	<i>Hbb-bs</i>	<i>Hbb-bs</i>	<i>Dpt</i>

Top 20 transcripts for each cell with a *Fap* sequencing count > 2. Original data from ¹.

Table S3. Pathway analyses of the selected transcripts from table S2.

Top 10 GOTERM_BP Term	P Value	Fold Enrichment	Bonferroni	Benjamini	FDR
GO:0006412~translation	3.99E-15	12.599311	1.90E-12	1.90E-12	5.72E-12
GO:0032496~response to lipopolysaccharide	8.19E-06	10.798447	0.003885	0.001944	0.011715
GO:0030199~collagen fibril organization	1.28E-05	34.091252	0.006081	0.002031	0.018358
GO:0007568~aging	4.33E-05	10.759436	0.020352	0.005127	0.061869
GO:0009612~response to mechanical stimulus	8.70E-05	21.104108	0.040482	0.008231	0.124299
GO:0009314~response to radiation	1.84E-04	35.454902	0.083596	0.014444	0.262405
GO:0042060~wound healing	4.09E-04	14.144243	0.176457	0.027353	0.582618
GO:0043206~extracellular fibril organization	7.28E-04	72.521390	0.292442	0.042320	1.035793
GO:0001649~osteoblast differentiation	8.19E-04	11.766007	0.322242	0.042298	1.163880
GO:0042989~sequestering of actin monomers	8.72E-04	66.477941	0.339104	0.040570	1.238798
Top 10 GOTERM_CC Term	P Value	Fold Enrichment	Bonferroni	Benjamini	FDR
GO:0005840~ribosome	2.15E-21	28.38738602	2.57E-19	2.57E-19	2.46E-18
GO:0031012~extracellular matrix	9.45E-21	20.06326531	1.13E-18	5.67E-19	1.08E-17
GO:0070062~extracellular exosome	5.39E-16	4.09668768	6.66E-14	2.22E-14	6.33E-13
GO:0022627~cytosolic small ribosomal subunit	2.45E-15	58.29703504	2.93E-13	7.33E-14	2.81E-12
GO:0005576~extracellular region	1.99E-13	4.806943199	2.38E-11	4.77E-12	2.28E-10
GO:0030529~intracellular ribonucleoprotein complex	4.76E-12	13.16651786	5.71E-10	9.52E-11	5.47E-09
GO:0005925~focal adhesion	6.88E-11	10.77566679	8.25E-09	1.18E-09	7.90E-08
GO:0005615~extracellular space	1.07E-10	4.668977964	1.29E-08	1.61E-09	1.23E-07
GO:0022625~cytosolic large ribosomal subunit	3.07E-08	24.69324961	3.69E-06	4.10E-07	3.53E-05
GO:0005578~proteinaceous extracellular matrix	1.55E-06	8.888788427	1.86E-04	1.86E-05	0.001782
GO:0015935~small ribosomal subunit	3.09E-06	48.42857143	3.70E-04	3.37E-05	0.003544
Top 10 GOTERM_MF Term	P Value	Fold Enrichment	Bonferroni	Benjamini	FDR

GO:0003735~structural constituent of ribosome	4.48E-20	20.651042	5.82E-18	5.82E-18	5.21E-17
GO:0044822~poly(A) RNA binding	6.98E-09	4.898360	9.08E-07	4.54E-07	8.13E-06
GO:0019843~rRNA binding	2.67E-05	28.395182	0.003461	0.001155	0.031050
GO:0003729~mRNA binding	1.60E-04	11.518046	0.020602	0.005191	0.186307
GO:0005518~collagen binding	0.001263	18.480932	0.151523	0.032328	1.461140
GO:0005201~extracellular matrix structural constituent	0.009613	19.945884	0.715115	0.188831	10.638815
GO:0008201~heparin binding	0.017288	7.221026	0.896388	0.276657	18.379381
GO:0035662~Toll-like receptor 4 binding	0.017928	109.037500	0.904799	0.254701	18.996059
GO:0048306~calcium-dependent protein binding	0.025784	11.851902	0.966489	0.314303	26.228997
GO:0050786~RAGE receptor binding	0.028532	68.148438	0.976789	0.313613	28.616601

Top 10 UP_KEYWORDS Term	P Value	Fold Enrichment	Bonferroni	Benjamini	FDR
Ribosomal protein	2.15E-23	31.471588	2.50E-21	2.50E-21	2.46E-20
Ribonucleoprotein	6.32E-20	20.742638	7.33E-18	3.66E-18	7.21E-17
Secreted	2.12E-13	5.308146	2.46E-11	8.21E-12	2.42E-10
Extracellular matrix	4.44E-08	13.593048	5.15E-06	1.29E-06	5.06E-05
Acetylation	8.75E-07	2.759932	1.01E-04	2.03E-05	9.98E-04
Disulfide bond	3.23E-06	2.658563	3.74E-04	6.24E-05	0.003683
Signal	9.87E-05	2.039107	0.011380	0.001634	0.112503
Chemotaxis	2.06E-04	16.991310	0.023592	0.002980	0.234539
Pyrrolidone carboxylic acid	8.09E-04	21.656720	0.089582	0.010374	0.918799
Innate immunity	8.97E-04	7.952779	0.098838	0.010353	1.018331

Top 10 terms as indicated in the column titles: BP, biological process; CC, cellular component; MF, molecular function; UP, UniProtKB keywords.

Table S4. Primers used for qPCR.

Transcript	Forward (5' to 3')	Reverse(5' to 3')
<i>Acta</i>	CCAGAGCAAGAGAGGGATCCT	TGTCGTCCCAGTTGGTGATG
<i>Actb</i>	TGTTACCAACTGGGACGACA	GGGGTGTGAAGGTCTCAA
<i>B2m</i>	TTCTGGTGCTTGTCTCACTG	TATGTTCCGGCTTCCCATTCT
<i>Col1a1</i>	GCACGAGTCACACCGGAACT	AAGGGAGCCACATCGATGAT
<i>Col1a2</i>	CTACTGGTGAAACCTGCATCCA	GGGCGGGCTGTATGAG
<i>Col3a1</i>	TCCTGAAGATGTCGTTGATGTG	TTTTTGCAAGTGGTATGTAATGTTCTG
<i>Ctgf</i>	CACTCTGCCAGTGGAGTTCA	AAGATGTCATTGTCCCCAGG
<i>Cthrc1</i>	CGGGATGGATTCAAAGGGGA	CGTGAATGTACACTCCGCAAT
<i>Des</i>	CTCGGAAGTTGAGAGCAGAGA	GTGAAGATGGCCTTGGATGT
<i>Fn1</i>	ACTGGATGGGGTGGGAAT	GGAGTGGCACTGTCAACCTC
<i>Fn1</i>	ACTGGATGGGGTGGGAAT	GGAGTGGCACTGTCAACCTC
<i>Gfap</i>	CCTTCTGACACGGATTGGT	ACATCGAGATCGCCACCTAC
<i>Htra1</i>	GATCTTCCCTGCCCTTGGC	CTACACCAACCTGTGCCAGC
<i>Mgp</i>	AGGACTCCATGCTTTCGTGA	ACCCGAGACACCATGAAGAG
<i>Mgp</i>	AGGACTCCATGCTTTCGTGA	ACCCGAGACACCATGAAGAG
<i>Mmp13</i>	TTGCCCTGGGAAGGAGAGA	AGTCCAGCTCAACAAGAAGAAGGT
<i>Mmp14</i>	AGTCAGGGTCACCCACAAAGA	TTTGGGCTTATCTGGGACAGA
<i>Mmp2</i>	ACCACCTTAACTGTTGCTTTTG	AGGAAATGCAGTGGAGTGGA
<i>Mmp3</i>	GGAGCTAGCAGGTTATCCTAAAAGC	TAGAAATGGCAGCATCGATCTTC
<i>Mmp7</i>	GGTGAGGACGCAGGAGTGAA	GAAGAGTGAAGCAAGCAAGGA
<i>Mmp8</i>	AAAAGGGAAGCTCAGTCTGTATACTC	AGAGGGCTGCAGAGTTAGTTACCA
<i>Mmp9</i>	GGACGACGTGGGCTACGT	CACGGTTGAAGCAAGCAAGGA
<i>Npc2</i>	TTGTGCAGCTGACAGGGAT	CCCCTGCACTTCAAGGACT
<i>Npc2</i>	TTGTGCAGCTGACAGGGAT	CCCCTGCACTTCAAGGACT
<i>Ppib</i>	CAGGGGAGATGGCACAGGAG	CGGCTGTCTGTCTTGGTGCTCTCC
<i>Reln</i>	ACATGAGAGGCCACCACACT	CTTCTCAGAGCATTGGAGGC
<i>Serpine1</i>	TTGTCCAGCGGGACCTAGAG	AAGTCCACCTGTTTCACCATAGTCT
<i>Tgfb1</i>	CAACCCAGGTCTTCCCTAAA	GGAGAGCCCTGGATACCAAC
<i>Tgfb1</i>	CAACCCAGGTCTTCCCTAAA	GGAGAGCCCTGGATACCAAC
<i>Thbs2</i>	AGTGCACAGCTACAGCCTGA	ACAGAGTACTGGCGTCGGTC
<i>Thbs2</i>	AGTGCACAGCTACAGCCTGA	ACAGAGTACTGGCGTCGGTC
<i>Timp1</i>	CCTTCGCATGGACATTATTCTC	TCTCTAGGAGCCCCGATCTG
<i>Vim</i>	GGATTCCACTTCCGTTCAA	GAAATTCAGGAGGAGATGC

Supplementary References

1. Gu W, Ni Z, Tan YQ, Deng J, Zhang SJ, Lv ZC, Wang XJ, Chen T, Zhang Z, Hu Y, Jing ZC, Xu Q. Adventitial Cell Atlas of wt (Wild Type) and ApoE (Apolipoprotein E)-Deficient Mice Defined by Single-Cell RNA Sequencing. *Arterioscler Thromb Vasc Biol* 2019;**39**:1055-1071.

Figure 4E

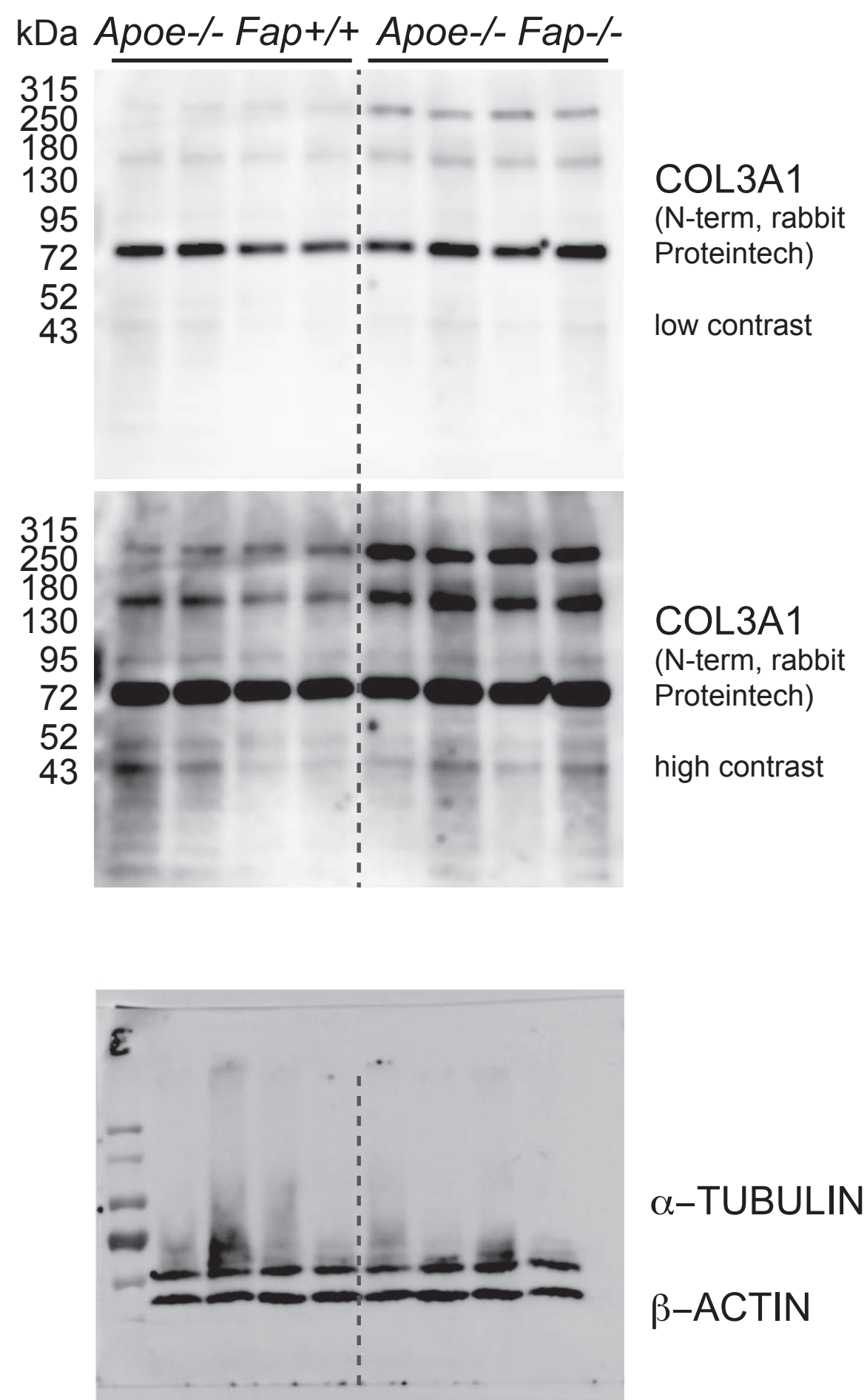


Figure S7A

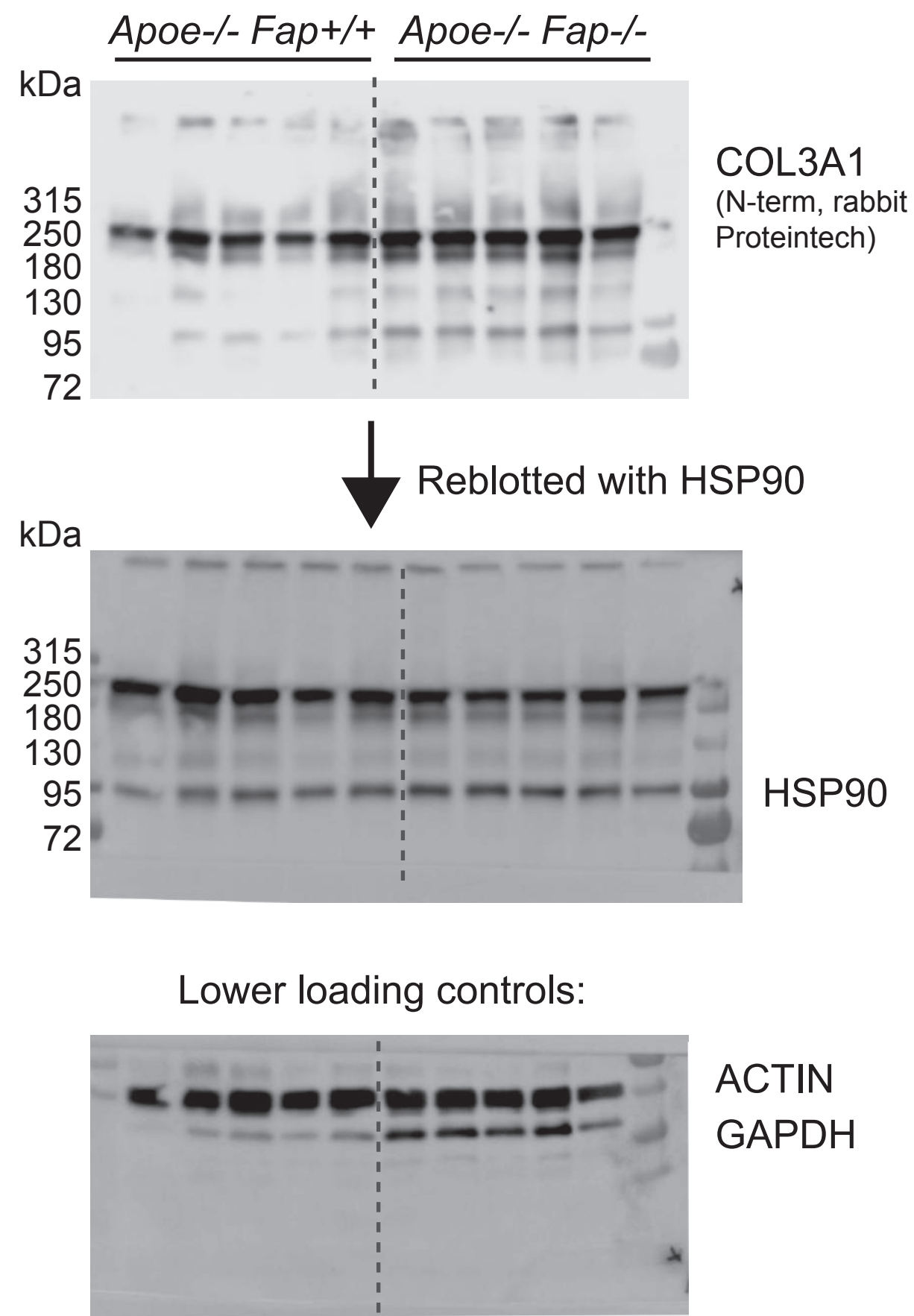


Figure S7C & E

